

## Energetics of lateral eddy diffusion/advection: Part II. Numerical diffusion/diffusivity and gravitational potential energy change due to isopycnal diffusion

HUANG Rui Xin<sup>1</sup>\*

<sup>1</sup>Department of Physical Oceanography, Woods Hole Oceanographic Institution, Woods Hole 02543-1050, USA

Received 30 August 2013; accepted 17 December 2013

©The Chinese Society of Oceanography and Springer-Verlag Berlin Heidelberg 2014

### Abstract

Study of oceanic circulation and climate requires models which can simulate tracer eddy diffusion and advection accurately. It is shown that the traditional Eulerian coordinates can introduce large artificial horizontal diffusivity/viscosity due to the incorrect alignment of the axis. Therefore, such models can smear sharp fronts and introduce other numerical artifacts. For simulation with relatively low resolution, large lateral diffusion was explicitly used in models; therefore, such numerical diffusion may not be a problem. However, with the increase of horizontal resolution, the artificial diffusivity/viscosity associated with horizontal advection in the commonly used Eulerian coordinates may become one of the most challenging obstacles for modeling the ocean circulation accurately. Isopycnal eddy diffusion (mixing) has been widely used in numerical models. The common wisdom is that mixing along isopycnal is energy free. However, a careful examination reveals that this is not the case. In fact, eddy diffusion can be conceptually separated into two steps: stirring and subscale diffusion. Due to the thermobaric effect, stirring, or exchanging water masses, along isopycnal surface is associated with the change of GPE in the mean state. This is a new type of instability, called the thermobaric instability. In addition, due to cabbeling subscale diffusion of water parcels always leads to the release of GPE. The release of GPE due to isopycnal stirring and subscale diffusion may lead to the thermobaric instability.

**Key words:** Eulerian coordinates, numerical diffusivity, numerical dissipation, energetics of isopycnal eddy diffusion

**Citation:** Huang Rui Xin. 2014. Energetics of lateral eddy diffusion/advection: Part II. Numerical diffusion/diffusivity and gravitational potential energy change due to isopycnal diffusion. *Acta Oceanologica Sinica*, 33(3): 19–39, doi: 10.1007/s13131-014-0410-0

### 1 Introduction

For more than 200 years, both the Eulerian and Lagrangian coordinates have been used in fluid dynamics extensively. Most currently used numerical models are based on the Eulerian coordinate. Most people believe that these two coordinate systems should be equivalent. As such, results obtained from one system can be readily transformed into the other coordinates. However, this equivalence had not been proved mathematically for a long time. The first step was taken by Wegner (1987), who showed that for one-dimensional flow of gas dynamics, the weak solutions (weak solutions contain discontinuity in the derivatives of the solutions) obtained from these two coordinate systems is equivalent, i.e., there exists a one-to-one map between these two sets of weak solutions. This discovery reaffirmed people's belief.

However, further studies indicated that this is not the case. In fact, Hui and his colleagues showed that for two-dimensional and three-dimensional flows, these two systems are not equivalent to each other theoretically, e.g., Hui et al. (1999), Hui and Kudriakov (2001), Hui (2007). For example, in mathematical terms, gas dynamical equations for two-dimensional and three-dimensional flows in Eulerian coordinates are strongly hyperbolic; on the other hand, the corresponding equations in the Lagrangian coordinates are weakly hyperbolic. In particular, the Cauchy problem for strongly hyperbolic system is well-posed in

the sense of Hadamard; however, weakly hyperbolic system is not well posed in the sense of Hadamard; it is weakly well-posed only in a weaker sense (Hui and Xu, 2012).

A better understanding of the meaning of such mathematical theory may take some time for oceanographers and numerical modelers. However, a simple take home message may be as follows. First, simple one-to-one mapping between Eulerian coordinate and Lagrangian coordinates may not exist. Second, parameterization of models based on these two coordinate systems can be quite different. In particular, Lagrangian diffusivity inferred from drifters may not be simply applied for models based on Eulerian coordinates. Thus, the high value of Lagrangian diffusivity inferred from drifters and floats may not be applicable to numerical models based on Eulerian coordinates.

Although the Eulerian coordinates have a great advantage for numerical simulation, there are many problems associated with lateral advection and diffusion. In particular, models based on the Eulerian coordinates have difficulties in dealing with high concentration gradient because of numerical dispersion. Numerical dispersion in the Eulerian coordinates sometime appears in forms similar to physical dispersion; however, such dispersion is entirely due to the numerical errors. The existence of numerical dispersion can lead to smearing of tracer fronts. Although using high-order finite difference schemes can reduce the amount of the smearing, it can also bring about artificial oscil-

\*Corresponding author, E-mail: [rhuang@whoi.edu](mailto:rhuang@whoi.edu)

lations of the solutions (Spivakovskaya et al., 2007; Zhang and Wang, 1999).

Isopycnal analysis has been a commonly used approach and the common wisdom is that isopycnal mixing is free of energy. This is a statement often encountered in oceanographic literature; however, such a statement is without solid and careful proof. We will go through careful examination of isopycnal eddy diffusion (mixing). First of all, eddy diffusion along isopycnal surface can be conceptually separated into two stages, stirring and subscale diffusion. The second stage, subscale diffusion, is always associated with GPE release. We will show that in the first stage, isopycnal stirring, GPE of the system can be changed, either increased or reduced. The change of GPE during isopycnal stirring is closely linked to the gradient of elasticity on isopycnal surface. Due to the horizontal variation of elasticity on isopycnal surface, lateral adiabatic stirring of water parcels always leads to change of GPE. In addition, GPE is reduced during the second stage, subscale diffusion. Thus, isopycnal eddy diffusion is not energy free, and energetics of isopycnal eddy diffusion should be carefully analyzed.

## 2 Numerical diffusivity/viscosity induced by horizontal advection in the Eulerian coordinates

### 2.1 Simple examples of numerical diffusion in Eulerian coordinates

It is well-known that the advection terms in Eulerian models can introduce numerical diffusion and other errors. To demonstrate this point, we first show the simple case with pure diffusion. The model has horizontal grid size of  $\Delta x = \Delta y = 100$  m. At time  $T_0 = 0$ , the tracer concentration is set to  $C = 1$  at a grid point at the origin of the coordinates, but there is no tracer at any other points. The diffusivity is set to  $k = 35$  m<sup>2</sup>/s and the time step is  $\Delta t = 1$  s. After 1 000 time steps, the tracer is spread into a large area, with the maximum of  $C = 0.0236$ , shown as Fig. 1.

As the next step, we show that advection term in the Eulerian

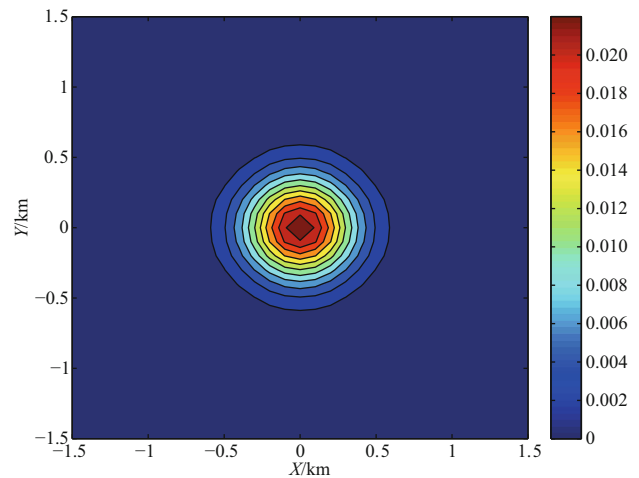


**Fig. 1.** Tracers spreading due to pure diffusion ( $k = 35$  m<sup>2</sup>/s,  $T = 1\,000$  s,  $C_{\max} = 0.0236$ ).

coordinates can induce numerical diffusion. It is well known that tracer conservation equation in the Lagrangian coordinates does not explicitly include the diffusion associated with advection.

To begin with, we start with a one-dimensional case. As shown by the heavy line bars in Fig. 2, after 1 000 time steps, the tracer patch moves to 1 km east of the origin. Tracer is all confined in a single grid box, so that the concentration is still equal to one unit.

However, we can also simulate the tracer concentration using the Eulerian coordinates. First, for the case with advection only, we can use upwind scheme or central difference scheme. After 1 000 time steps, the tracer concentration is shown as blue curves in Fig. 2. It is clear that due to numerical errors, tracer is spreading along the path. The upwind scheme is more diffu-

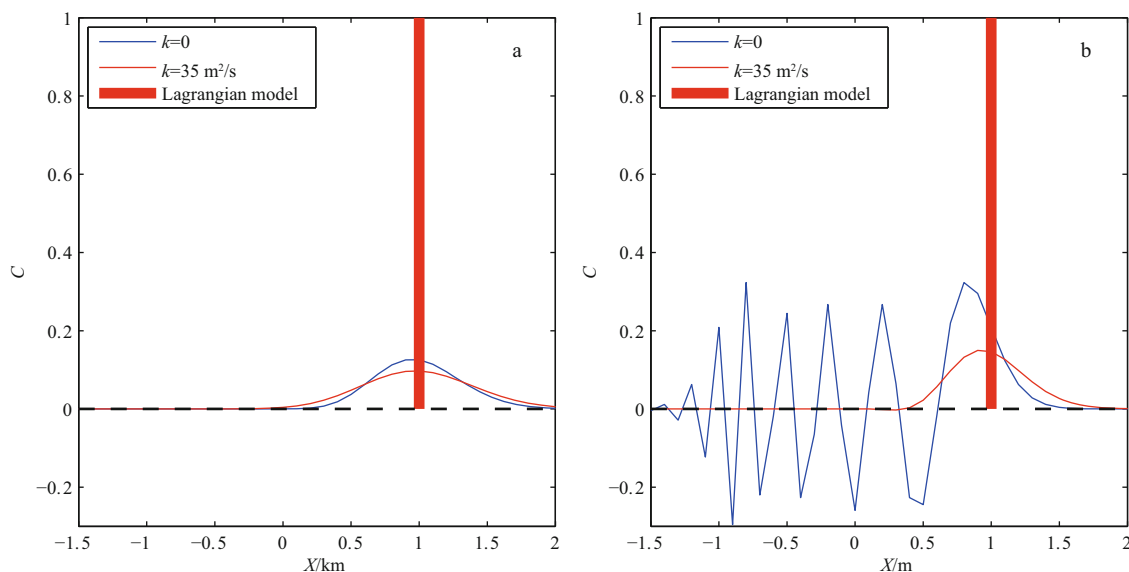


**Fig. 2.** Tracer spreading in a one-dimensional model due to advection and diffusion, ( $u = 1$ ,  $T = 1\,000$  s) based on the upwind scheme (a) and central difference scheme (b).

sive than the central difference scheme; however, the later can introduce oscillations, as shown in Fig. 2b. Adding the lateral diffusion enhances the lateral spreading of tracer; in addition, it smoothes the oscillatory behavior of the solution, Fig. 2b. For the one-dimensional case discussed here, it is possible to further reduce the numerical errors introduced in the Eulerian coordinates by using more advanced finite difference schemes, e.g., Hui and Xu (2012).

We now discuss the two-dimensional case. The results obtained by the upwind scheme and central difference scheme, with or without diffusion, are shown in Fig. 3. As in the one-dimensional case, pure advection can introduce numerical diffusion, left panels of Fig. 3. In this two-dimensional case, there are again the oscillations. Nevertheless, the spreading of tracer due to advection is clearly shown in this figure. Adding diffusion can smooth out the oscillations.

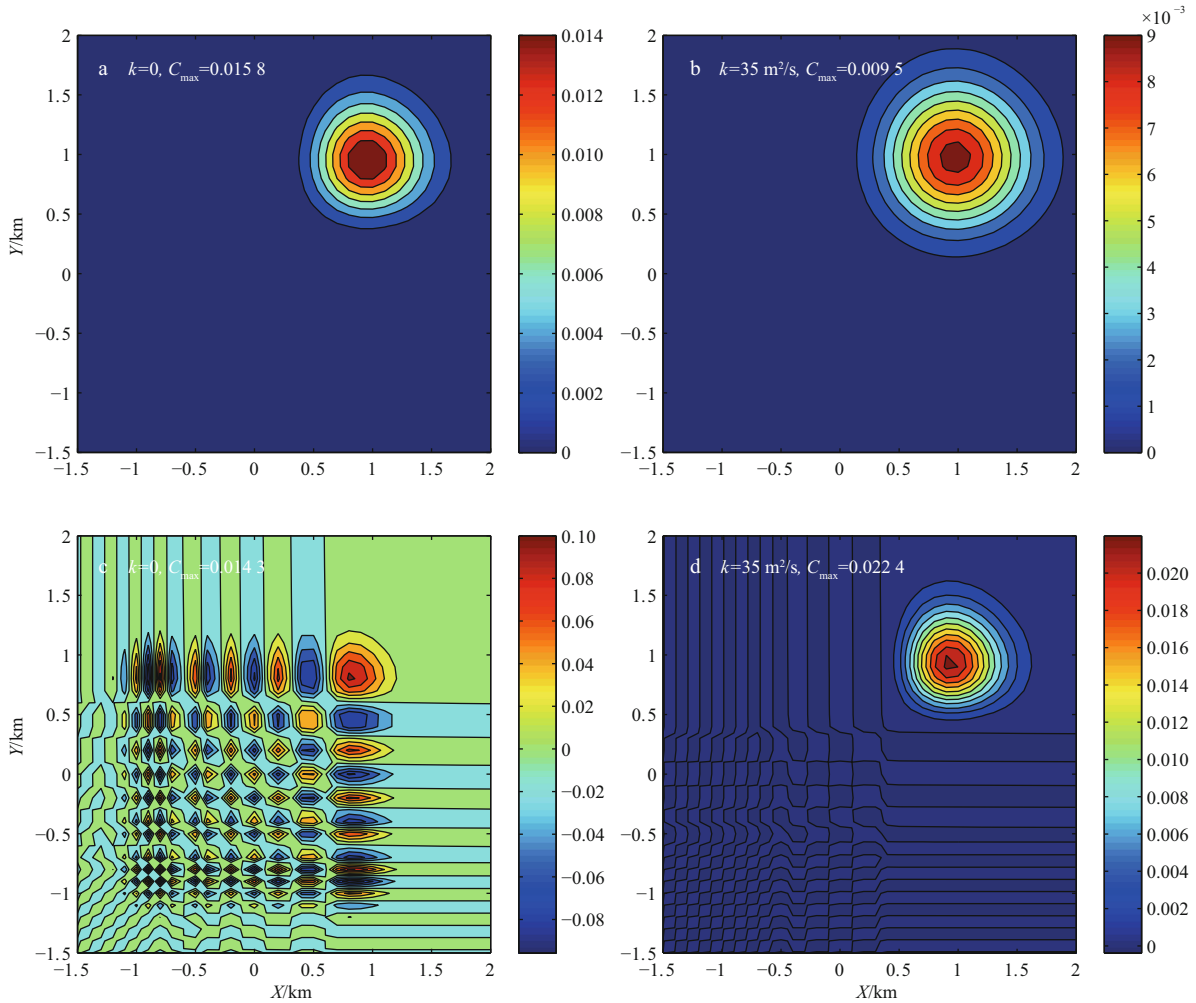


**Fig.3.** Tracer spreading (two-dimensional model) due to advection and diffusion. a and c for advection only; b and d for advection and diffusion; a and b for upwind scheme; c and d for central difference scheme.

## 2.2 Artificial diffusivity due to horizontal advection in Eulerian coordinates

### 2.2.1 The special case of 45° off the horizontal axis

The numerical error associated with horizontal advection terms in the Eulerian models can be demonstrated with the following simple case. Assume that at a given grid point in the two-dimensional plane, water flows with velocity  $U$ , as shown in Fig. 4a. To illustrate the numerical artifact associated with the Eulerian coordinates, we choose two sets of coordinates and compare the difference in the lateral advection terms simulated in these two coordinates. In the Eulerian coordinates labeled by  $(X, Y)$ , the local  $X$ -axis is aligned with the flow velocity  $U$ . In the

Eulerian coordinates labeled by the lower case characters  $(x, y)$ , the  $x$ -axis is 45° off the  $U$  vector. This case represents the worst situation for the artificial diffusivity induced by horizontal advection in the Eulerian coordinates. Let us examine salinity balance at grid point 5.

For comparison, our analysis below will be based on the commonly used central finite difference scheme, which will be used for both coordinates. Ideally, the contribution due to lateral advection should be the same in these two sets of coordinates, i.e., at each time step the contribution associated with lateral advection should be independent of the choice of coordinates, such as the orientation of the axis. However, as will be shown shortly, this is not the case.

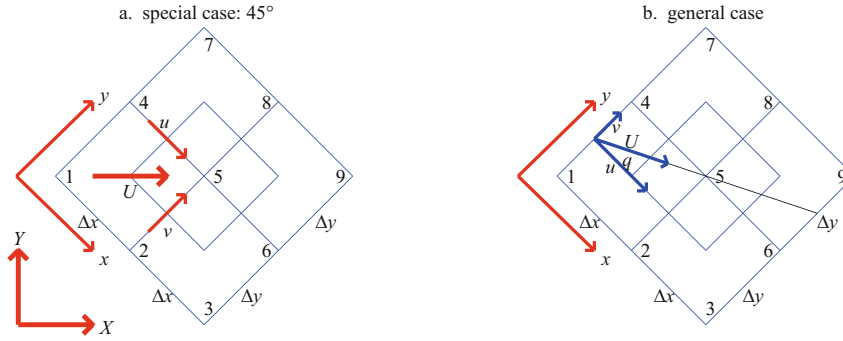


**Fig.4.** A standard grid used in an Eulerian coordinates.

We will be focused on a two-dimensional flow with no source or sink, i.e., the velocity field is divergence free. From the construction of these two coordinate systems, it is clear the velocity components and grid size satisfy the following constraints

$$U = \sqrt{2}u = \sqrt{2}v; \Delta X = \Delta Y = \sqrt{2}\Delta x = \sqrt{2}\Delta y. \quad (1)$$

Let us consider the following two-dimensional salinity balance equation

$$\frac{\partial S}{\partial t} = -\nabla \cdot (\bar{u}S) + K_H \nabla^2 S. \quad (2)$$

Salinity change due to lateral advection in grid point 5 can be written in finite difference form in coordinate  $x$ - $y$  as follows. Salinity flux associated with  $u$ -velocity component flows from grid point 4 to grid points 5 and 6; similarly, salinity flux associated with  $v$ -velocity component flows from grid point 2 to grid points 5 and 8. Using central difference scheme, we have

$$\begin{aligned} -\nabla \cdot (\bar{u}S) &= 0.5u[(S_4 + S_5) - (S_5 + S_6)] / \Delta y + \\ &\quad 0.5v[(S_2 + S_5) - (S_5 + S_8)] / \Delta y \\ &= 0.5u[S_2 + S_4 - S_6 - S_8] / \Delta y. \end{aligned} \quad (3)$$

On the other hand, the corresponding advection term calculated in the  $X$ - $Y$  coordinate has no contribution from the lateral grid points 3 and 7. With the only contribution from the upstream and downstream grids, the lateral advection term is

$$\begin{aligned} -\nabla \cdot (\bar{U}S) &= 0.5U[(S_1 + S_5) - (S_5 + S_9)] / \Delta X \\ &= 0.5U[S_1 - S_9] / \Delta Y \\ &= 0.5u(S_1 - S_9) / \Delta x. \end{aligned} \quad (4)$$

Note that in the derivation above, we have used the Eq. (1).

It is clear that salinity change due to horizontal advection in these two coordinates is different. From the physical point of view, contribution of the horizontal advection to the salinity at a given grid point should have a single value, independent of the choice of the coordinates. In the present cases, we have two different values. Thus, there are only two possible cases: (1) both of them are wrong; (2) one of them is correct or a much better choice, and the other one is wrong or a bad choice.

In this study, we will take the expression in Eq. (4) as the

“truth”, and the difference between the advection terms calculated in  $x$ - $y$  coordinates and the  $X$ - $Y$  coordinates is defined as the artificial diffusivity due to advection in Eulerian coordinates. It is clear that numerical artifact defined in this way may depend on the choice of finite difference scheme. However, we believe that although the choice of the finite difference scheme can affect the results to certain degree, the artificial eddy diffusivity associated with the Eulerian coordinates is intrinsic to this coordinates system.

We further quantify this error in terms of an equivalent Laplacian diffusivity  $\tilde{K}_H$ . Note that in the  $x$ - $y$  coordinates, salinity change due to Laplacian diffusion can be written in terms of second-order finite difference

$$K_H \nabla^2 S = K_H (S_2 + S_4 + S_6 + S_8 - 4S_5) / \Delta x^2. \quad (5)$$

Hence, in the  $x$ - $y$  coordinates the artificial diffusivity associated with the advection terms can be quantified in terms of an equivalent Laplacian eddy diffusivity  $\tilde{K}_H$  defined through the following formula

$$\begin{aligned} &\frac{U}{2\sqrt{2}\Delta x} [S_2 + S_4 - S_6 - S_8 - (S_1 - S_9)] \\ &= \frac{\tilde{K}_H}{\Delta x^2} (S_2 + S_4 + S_6 + S_8 - 4S_5). \end{aligned} \quad (6)$$

As a result, the equivalent numerical diffusivity due to horizontal advection in the Eulerian coordinates is defined by

$$\tilde{K}_H = F \cdot R, \quad F = U\Delta x, \quad R = \frac{S_2 + S_4 - S_6 - S_8 - S_1 + S_9}{2\sqrt{2}(S_2 + S_4 + S_6 + S_8 - 4S_5)}. \quad (7)$$

Note that in this way, factor  $F$  is a parameter of the model resolution and the local velocity, but the factor  $R$  depends on the tracer salinity only, with nothing to do with the flow velocity and grid size.

Since Eq. (7) is homogeneous in its variables, we introduce a set of non-dimensional and normalized variables

$$S_i = \bar{S} + \Delta S \cdot S'_i, \quad i=1,2,\dots,9, \quad (8)$$

where  $\bar{S}$  and  $S'_i$  are the local mean salinity and the new non-

dimensional salinity variable. Substituting Eq. (8) into Eq. (7) and dropping the primes, we have a relation based on normalized variables

$$R = \frac{S_2 + S_4 - S_6 - S_8 - S_1 + S_9}{2\sqrt{2}D}, D = S_2 + S_4 + S_6 + S_8 - 4S_5. \quad (9)$$

Because this formula is a function of the normalized salinity with the local mean salinity removed, we can assume that the normalized salinity in each grid point is completely random and calculate the corresponding factor  $R$ . Since a very small factor  $D$  can lead to an extremely large factor  $R$  and thus an extremely large equivalent diffusivity, we will set a lower bound for the absolute value of  $D$  as follows

$$\begin{aligned} & \text{if } D_{\text{limit}} > D > 0, \text{ then } D = D_{\text{limit}}; \\ & \text{if } -D_{\text{limit}} < D < 0, \text{ then } D = -D_{\text{limit}}. \end{aligned} \quad (10)$$

Choosing value of  $D_{\text{limit}}$  for  $10^{-5}$  to  $10^{-4}$  gives solutions in similar range.

Factor  $R$  is calculated using a Monte-Carlo method as follows. Each time we can use a standard subroutine in Matlab to generate a series of random number for salinity ( $S_i, i=1,2,\dots,9$ ).  $R$  can be calculated from Eq. (9). 101 sets of experiments were carried out and each set includes total number  $\text{Imt}=5\,000\,000$  series of salinity. A typical output from these runs is shown in Fig. 5. Since the equivalent diffusivity can be positive or negative, we separate them into the corresponding positive bin and negative bin; the corresponding mean of the positive/negative values are calculated accordingly.

From this example, the amplitude of the mean equivalent factor is approximately 1.8. Although, such mean can vary due to the random nature of this factor and for different choice of  $D_{\text{limit}}$ , we will use 1.8 as a typical value for our discussion below. The probability of generating equivalent positive or negative diffusivity is the same, i.e., 50%, as indicated by the heavy dashed line in Fig. 5. As will be discussed below, a negative value of  $R$  indicates anti-diffusion, or demixing, which is a non-physical phenomenon intrinsic to the lateral advection term simulated in the traditional Eulerian coordinates.

### 2.2.2 The general case of arbitrary velocity angle

In the derivation above, we assume the worst case, i.e. when the velocity is  $\theta=45^\circ$  off the  $x$ -axis. For the general case, the velocity vector angle  $\theta$  is smaller than  $45^\circ$ , as shown in Fig. 4b by the blue vectors. The advection term in the  $x$ - $y$  coordinates is

$$\begin{aligned} -\nabla \cdot (\bar{u}\bar{S}) &= 0.5u[(S_4 + S_5) - (S_5 + S_6)] / \Delta x + \\ & 0.5v[(S_{2n} + S_5) - (S_5 + S_{8n})] / \Delta x \\ &= 0.5u[S_4 - S_6] / \Delta x + 0.5v[S_{2n} - S_{8n}] / \delta y. \end{aligned} \quad (3')$$

From Fig. 4b, we have the following relations:

$$\begin{aligned} u &= U \cos \theta, v = U \sin \theta; \\ \delta y &= \Delta y \tan \theta, S_{2n} - S_{8n} = (S_2 - S_8) \tan \theta; \\ -\nabla \cdot (\bar{u}\bar{S}) &= 0.5U[\cos \theta(S_4 - S_6) + \sin \theta(S_2 - S_8)] / \Delta x. \end{aligned} \quad (3'')$$

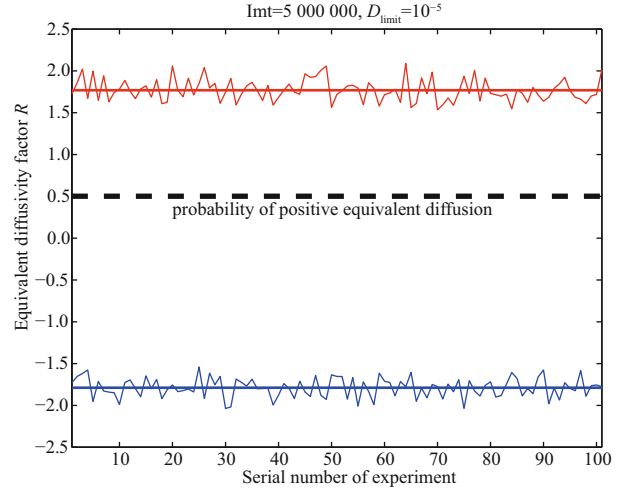


**Fig. 5.** Equivalent diffusivity factor  $R$  inferred from a set of Monte-Carlo experiments.

The corresponding advection term calculated in the  $X$ - $Y$  coordinate is

$$\begin{aligned} -\nabla \cdot (\bar{U}\bar{S}) &= 0.5U(S_{1n} - S_{9n}) / \delta Y \\ &= 0.5U\{[S_4 + (S_1 - S_4)\tan \theta] - [S_6 + (S_9 - S_6)\tan \theta]\} / \delta Y. \end{aligned} \quad (3''')$$

where  $\delta Y = \Delta x / \cos \theta$  is the corresponding grid size in the direction following the flow.

$$-\nabla \cdot (\bar{U}\bar{S}) = 0.5U[(S_4 - S_6)\cos \theta + (S_1 + S_6 - S_4 - S_9)\sin \theta] / \Delta x. \quad (5)$$

Here again, we define the difference between the advection term calculated in  $x$ - $y$  coordinates and the  $X$ - $Y$  coordinates as the artificial diffusivity introduced through the lateral advection terms in Eulerian coordinates. We further quantify this error in terms of an equivalent Laplacian diffusivity  $\tilde{K}_H$

$$\begin{aligned} & \frac{U}{2\Delta x}[S_2 + S_4 - S_6 - S_8 - (S_1 - S_9)] \sin \theta \\ &= \frac{\tilde{K}_H}{\Delta x^2}(S_2 + S_4 + S_6 + S_8 - 4S_5). \end{aligned} \quad (6)$$

Therefore, the corresponding formula is

$$\tilde{K}_H = F \cdot R, F = U\Delta x, R = \frac{S_2 + S_4 - S_6 - S_8 - S_1 + S_9}{2(S_2 + S_4 + S_6 + S_8 - 4S_5)} \sin \theta. \quad (7')$$

The first factor in  $R$  can be calculated through the Monte-Carlo experiment as discussed above. Using the results shown in Fig. 5, the corresponding factor of  $R$  in Eq. (7') can be calculated, and the result is shown in Fig. 6.

Using the 50-year mean velocity data from SODA 2.1.6 (1958–2008; Carton and Giese, 2008), the root-mean-square horizontal velocity in the model ocean is on the order of 0.1 m/s in the upper ocean, and gradually decline to 0.01 m/s in the

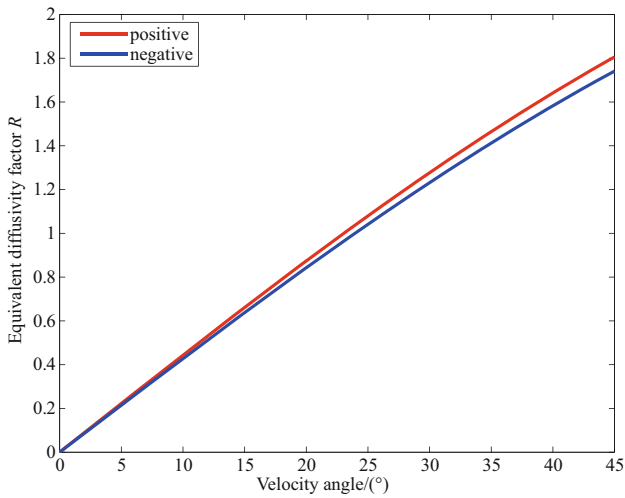


**Fig.6.** Equivalent diffusivity factor  $R$  as function of the velocity angle.

deep ocean. The corresponding mean velocity angle is in the range of  $30^{\circ}$ – $40^{\circ}$ . Accordingly, factor  $R$  is in the range of 1.2–1.4. Thus, as a slightly conservative estimate, we will assume

$$R \gg 1, \text{ and } \tilde{K}_H = F \cdot R \approx F = U \Delta x. \quad (7'')$$

Therefore, the artificial diffusivity induced by through the lateral advection term in the Eulerian coordinates can be estimated using the simple Eq. (7'').

2.2.3 *The equivalent diffusivity can be negative*

As shown in Fig. 5, the equivalent diffusivity due to horizontal advection can be negative. As an example, we show such a case in Fig. 8.

Assume that due to the time evolution and other dynamical

processes the non-dimensional normalized salinity distribution has the values shown in Fig. 8. We also assume that the velocity  $(u, v)$  is of one unit, so that the velocity is  $45^{\circ}$  rotated from the  $x$ -axis. The horizontal advection along the  $x$  and  $y$  axis all makes positive contribution

$$S_4 - S_6 = 0.5; S_2 - S_8 = 0.5.$$

Therefore, horizontal advection in the  $x$ - $y$  coordinates tends to increase salinity in grid Point 5.

On the other hand, however, contribution of horizontal advection in the  $X$ - $Y$  is negative

$$S_1 - S_9 = -0.05,$$

i.e., it tends to reduce salinity in grid point 5. Thus, horizontal advection term in  $x$ - $y$  coordinates has a sign opposite to that in the  $X$ - $Y$  coordinates, and it overpowers the advection term in  $X$ - $Y$  coordinates. On the other hand, the effect of pure diffusion in this case is negative

$$S_2 + S_4 + S_6 + S_8 - 4S_5 = -1.2,$$

i.e., the Laplacian diffusion tends to reduce salinity in grid Point 5. Thus, Laplacian diffusion in  $x$ - $y$  coordinates has the same sign as the horizontal advection in the  $X$ - $Y$  coordinates. On the other hand, horizontal advection terms in  $x$ - $y$  coordinates make a contribution opposite to that of horizontal diffusion. This phenomenon can be called “demixing”. Such demixing may be an artifact in the numerical model, and the reason of such problem may be linked to the incorrect orientation of the local coordinates and the central difference scheme used in the calculation.

As shown above, factor  $R$  is independent of the grid size and the amplitude of tracer anomaly. In fact, for the general case an angle equal or larger than  $25^{\circ}$ , the corresponding equivalent diffusion coefficient  $R$  is approximately 1. Thus, the factor calcu-

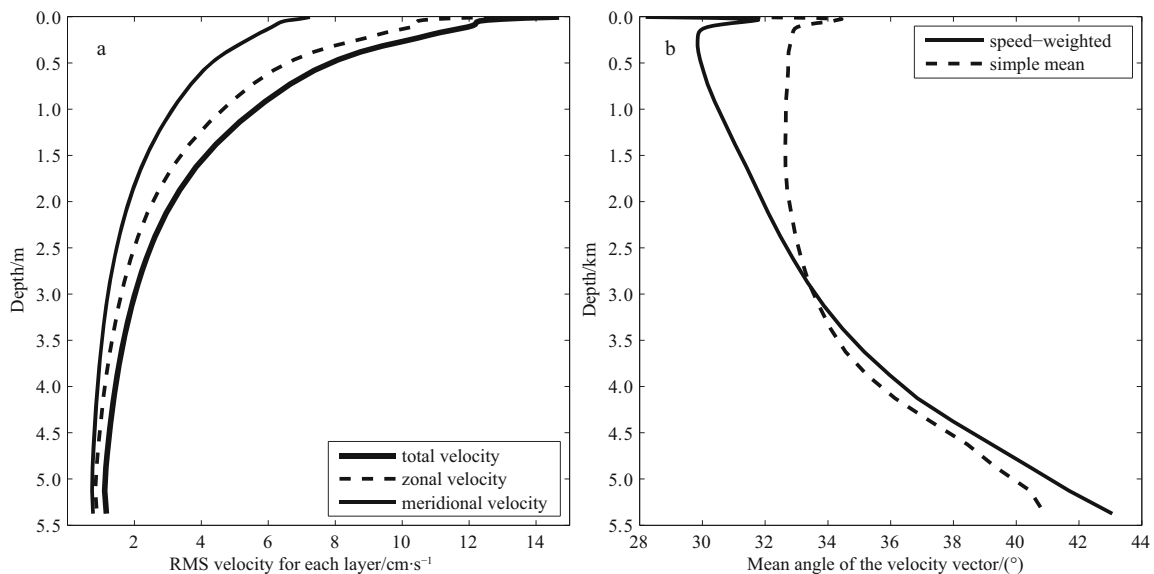


**Fig.7.** The mean velocity angle diagnosed from SODA data.

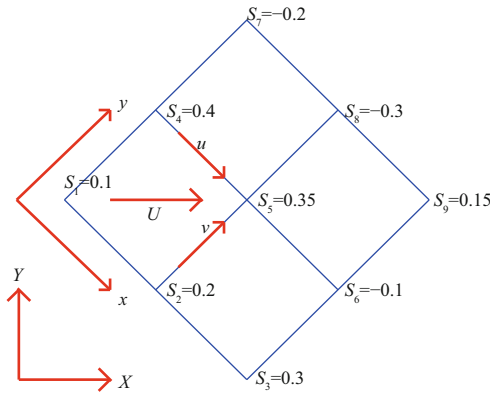


**Fig.8.** A case with negative equivalent diffusivity.

lated above can be applied to cases with resolution on the order of 100 km and down to horizontal grid size of 1 mm which represents the size of grid controlled by molecule diffusion.

**2.3 Comparing the equivalent diffusivity with observations**

According to Eq. (7''), artificial diffusivity is simply a product of speed and grid size. Assuming the mean velocity angle is 25°, the corresponding diffusivity as a function of the horizontal grid size is shown as the blue lines in Fig. 9. The black line represents the typical value of lateral diffusivity used in oceanic circulation models. For comparison, we also include the horizontal diffusivity observed in the ocean and plotted as the red lines in Fig.

9, taken from Obuko (1971) and Ledwell et al. (1998).

Note that lateral diffusion in the ocean depends on the horizontal scale of the phenomena. For horizontal scale on the order to 1 to 100 km, tracer can appear in forms of streakiness. Strong eddies tend to separate tracers into several patches which move in the ocean in forms of streak. The horizontal scale of streaks is on the order of eddy scale, i.e. on the order to 100 km. As Ledwell et al. (1998) pointed, for horizontal scale of 30–300 km the equivalent lateral diffusivity is approximately 1 000 m<sup>2</sup>/s. On the other hand, each streak of tracer has a typical width on the order of 10 km. Tracer in each patch spreading with a much smaller diffusivity. Ledwell et al. (1998) put the estimate for horizontal diffusion on horizontal scale of 1–10 km at the value of 2 m<sup>2</sup>/s.

In a recent study <sup>1)</sup>, tracer was released upstream of the Drake Passage as part of the diapycnal and isopycnal mixing experiment in the Southern Ocean (DIMES). As a major effort, tracer data collected through the field experiments was compared with numerical simulation of an oceanic general circulation model. The model is based on the MIT OGCM, in which horizontal vorticity is advected with a forth-order accurate spatial discretization using an enstrophy conserving and vector invariant formulation. Horizontal viscosity is biharmonic, which value scales according to local grid spacing and stresses. However, there is no explicit lateral diffusion of tracer. The meridional eddy diffusivity diagnosed from the model at 1500 m depth is 710 m<sup>2</sup>/s; on the upper kilometer, it is reduced to 300 m<sup>2</sup>/s. Tulloch et al.<sup>1)</sup> also claimed that the eddy diffusivity diagnosed from the numerical model agrees with the Lagrangian-

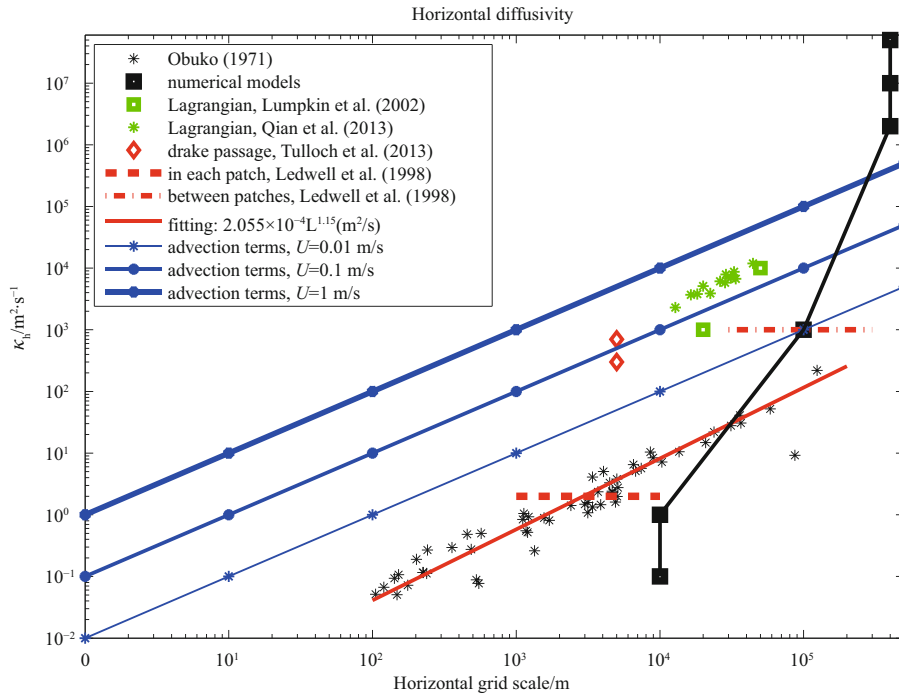


**Fig.9.** Lateral diffusion inferred from old tracer release experiments (black stars, the solid red line is a fitting line), recent tracer release experiments (red dashed lines) and Lagrangian drifters (green) vs lateral diffusivity used in numerical simulation (black) and artificial diffusion (blue lines) induced by advection in Euler coordinates. The red diamonds indicate the equivalent diffusivity diagnosed from a (1/20)° MIT model, with zero explicit lateral tracer diffusion.

<sup>1)</sup> Tulloch R, Ferrari R, Jahn O, et al. 2013. Direct estimate of lateral eddy diffusivity upstream of Drake Passage, manuscript

ian diffusivity inferred from the dispersion of approximately 50 acoustically tracked isopycnal floats, deployed on the same isopycnal surface as the tracer.

In general, diffusivity inferred from Lagrangian drifter and floats is much larger than that inferred from old tracer release experiments by Obuko (1971). For example, according to the study by Lumpkin et al. (2002), in the Gulf Stream the Lagrangian eddy length scale in the surface is in the range of 40–70 km. In the deep layer (averaged over 700 to 2 150 m), it is reduced to 5–20 km, much smaller than at the surface (Fig. 10).

The corresponding diffusivity in the Lagrangian coordinates is estimated at values much higher than that from the early tracer release experiments cited above, Fig. 11. For example, in the surface layer, the diffusivity is within the range of  $1 \times 10^3$ – $20 \times 10^3$   $\text{m}^2/\text{s}$ ; in the deep layer (around 1 500 m), it is 1 000  $\text{m}^2/\text{s}$ .

Similarly, Qian et al. (2013) analyzed the data collected in South China Sea, and their estimate is in the same range as that of Lumpkin et al. (2002).

At the early stage, with very limited computer power horizontal resolution for basin circulation or global circulation was on the order to  $4^\circ$ – $5^\circ$ . As an example, Bryan (1987) used  $4^\circ$  resolution in a sector model, and the typical value of horizontal diffusivity was set to  $10^7$   $\text{m}^2/\text{s}$ . Such a large diffusivity was used in order to stabilize the numerical simulation.

As the computer power increased, fine resolution has become accessible. For example, most climate-related simulations now are running on horizontal resolution on the order of  $1^\circ$ , or approximately 100 km, with typical horizontal diffusivity set to 1 000  $\text{m}^2/\text{s}$ , as shown in Fig. 9.

As the further increase of computer power, many high resolution models are now running with the horizontal diffusivity set to zero or a very small value, such as in the (1/6) $^\circ$  simulation of MIT ECCO2 and the more recent numerical experiments re-

ported by Tulloch et al. (2013). As shown in Fig. 9, for any given horizontal resolution, *in-situ* observations indicate that horizontal eddy diffusivity remains finite, not zero. Thus, a good numerical model should accurately simulate the lateral diffusion with such diffusivity. Putting the diffusivity zero in model implies that model is doing something unrealistic and we should try to avoid such cases.

On the other hand, however, setting the horizontal diffusivity to zero does not mean there is no horizontal diffusion in the model. In contrary, due to the nature of Eulerian coordinates, there is an artificial diffusion associated with the advection terms. According to Eq. (7''), for horizontal resolution of 10 km and very weak flow, on the order of 0.01 m/s, the artificial diffusivity is in the range of 100  $\text{m}^2/\text{s}$ . If the velocity is fast, in the range of 0.1 m/s, the corresponding artificial diffusivity is approximately 1 000  $\text{m}^2/\text{s}$ , which is much larger than the value of 10  $\text{m}^2/\text{s}$  inferred from observations. Similarly, if the model resolution is reduced to 1 km, observations indicate that the diffusivity is in the range of 1  $\text{m}^2/\text{s}$ , but the artificial diffusivity is in the range of 10–100  $\text{m}^2/\text{s}$ .

It is interesting to notice that the meridional eddy diffusivity diagnosed from the (1/20) $^\circ$  MIT model is fairly close to the prediction of the numerical diffusivity in the Eulerian models, assuming the mean velocity is about 0.1 m/s. Although many technical details of the MIT model are quite different from the simple central difference scheme used in our formulation, the corresponding eddy diffusivity does not seem much different from the expectation discussed above.

Note that even at the resolution of 1 mm, the corresponding artificial diffusivity can be as large as  $10^{-3}$   $\text{m}^2/\text{s}$ , which is 1 000 times larger than the molecular diffusivity. Thus, even for model run with such high-resolution, the output of the model may still be contaminated with the artificial diffusion.

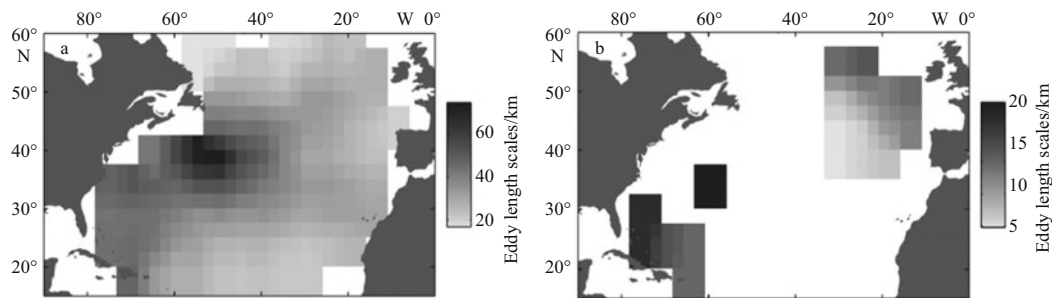


**Fig. 10.** Lagrangian eddy length scales observed by surface (a) and deep (b) drifters and floats (Lupkin et al., 2002).

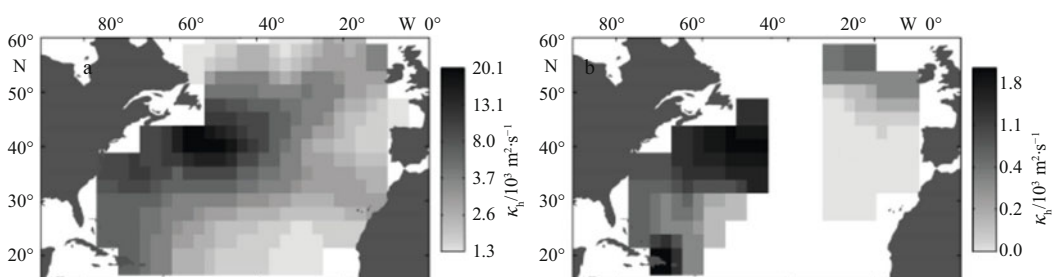


**Fig. 11.** Lagrangian eddy diffusivity inferred from drifters and floats in the North Atlantic Ocean (Lumpkin et al., 2002). a. Surface and b.  $z > 1500$  m.

#### 2.4 Artificial viscosity due to horizontal advection in Eulerian coordinates

Our discussion above is focused on the artificial diffusion for tracers, such as temperature and salinity. The basic idea also applies to the momentum equations. Before we start the analysis, it is worthwhile to emphasize that momentum dissipation and tracer diffusion may be governed by quite different physics. In most cases, momentum dissipation is linked to wave motions in the ocean, which can carry momentum over a large distance. On the other hand, tracer diffusion is linked to mass exchange due to turbulence motions, which can carry tracers over the length scale of eddies only.

Let us consider the following  $x$ -component momentum equation for a two-dimensional flow

$$\frac{\partial u}{\partial t} = -\nabla \cdot (\bar{u}u) + A_{m,h} \nabla^2 u . \quad (11)$$

Since we are concentrated on the horizontal aspect of the problem, other terms are omitted in the equation above. In this formula,  $A_{m,h}$  is the horizontal viscosity specified a priori. Note that in many models, other forms for this term can be used. However, we will use this form for simplicity.

Equation (11) looks quite similar to Eq. (2), with a minor difference. In fact, in most cases velocity at the vicinity of a grid point can be separated into two components, the mean velocity of the large scale flow and the local deviation from the mean:  $u=U+u'$ , where  $U=U(\xi, \eta)$ , is a slowly varying function of large-scale coordinates  $(\xi, \eta)$ . For a local grid, we treat this slowly varying function as a constant,  $U(\xi, \eta)=\text{constant}$ . For simplicity, we will drop the prime in the following analysis. In general, the local perturbations are much smaller than the large scale mean, i.e.,  $|u'| \ll |U|$ . Through linearization, this equation can be reduced to the following form

$$\frac{\partial u}{\partial t} = -\nabla \cdot (2\bar{U}u) + A_{m,h} \nabla^2 u . \quad (12)$$

Therefore, the  $u$ -momentum equation has almost exact form as the tracer equation, except the equivalent mean velocity should be doubled. From Eq. (12), one can derive the same conclusion for the artificial dissipation as before, plus an additional factor of 2. Note that, such artificial viscosity can be negative, i.e. it is equivalent to a negative viscosity. However, such a negative viscosity may be quite different from the equivalent negative viscosity associated with the backward cascade observed in quasi two-dimensional turbulence.

Accordingly, the blue lines in Fig. 9 also apply to the artificial momentum viscosity due to the horizontal advection in Eulerian coordinates, plus an additional factor of 2. There is, unfortunately, no reliable estimate of lateral momentum rate from observations; thus, a complete comparison in parallel is not possible at this time. However, it is to emphasize that the artificial momentum viscosity in Eulerian models can be quite large, and with either positive or negative signs. It is thus speculated that eddies obtained through the so-called eddy-resolving model based on the Eulerian coordinates may be contaminated by such random artificial dissipation at the length scale determined by the grid size.

#### 2.5 Remark

As numerical modeler, we are facing a grand challenge.

Since 1990 the most important progresses in numerical simulation are as follows. First, it was realized the large horizontal diffusivity may introduced unwanted diffusion in the diapycnal direction; thus, rotating of mix tensor has been widely used in basin-scale simulation, and the so-called neutral surface (McDougall, 1987a) has been introduced. Second, for model running with relatively low resolution on the order of  $1^\circ$ , the GM90 scheme (Gent and McWilliams, 1990) has been widely used for eddy parameterization. However, for the high resolution simulations the horizontal diffusivity is set to zero, so that these traditional techniques become outdated, and we are facing the challenge what to do next. The most important challenges now facing us are as follows.

Artificial tracer diffusion and momentum dissipation exist in the commonly used Eulerian models. Although using different finite difference schemes may reduce such errors, they are intrinsic to the Eulerian models. Therefore, it is desirable to develop new models in which the unwanted artificial diffusion/dissipation associated with the lateral advection in the traditional Eulerian coordinates can be substantially reduced or even completely avoided. The newly developed Hui transformation (Hui and Xu, 2012) may be one of the best ways to establish the next generation of ocean models.

Although most people believe that Eulerian and Lagrangian coordinates are equivalent, recent advance in mathematics showed that they are not equivalent. Thus, we face a grand challenge of revealing the difference between these two systems and we may have to start from zero and re-examine whether the conversion between these two systems used in previous oceanographic studies are valid or not.

We need to explore the nature of lateral eddy diffusion in the ocean models. It is now widely accepted that mechanical energy is one of the critical constraints for sub-grid scale parameterization. Recently, many studies explored the parameterization of vertical eddy diffusion based on external mechanical energy as integral constraint. One of our goal in this study is to explore using the external energy as an integral constraint for lateral eddy diffusion and lateral advection. In this section, we postulate to quantify the numerical errors associated with the horizontal advection terms in the Eulerian coordinates, we will further examine this problem in this study. In particular, we will quantify the GPE source/sink associated with lateral diffusion and advection in three commonly used vertical coordinate systems.

### 3 Gravitational potential energy change due to isopycnal diffusion

Although isopycnal mixing or mixing tensor rotation has been widely used in numerical models, some aspects of this problem have not been examined carefully. In most cases, the reason of using isopycnal mixing has been claimed as energy free. This is not an accurate statement. In this section, we will go through lateral diffusion along isopycnal surface carefully; in particular, we will examine the potential change of gravitational potential energy associated with isopycnal diffusion.

This section is organized as follows. In Section 3.1 we argue that the ocean is a continuous media; thus, one cannot talk about the consequence of moving a single water parcel alone; instead, it is more meaningful to discuss the consequence of exchanging water parcels. Due to the thermobaricity, lateral exchange of water parcels can lead to release of GPE, and this is called the thermobaric instability, which will be discussed

in Section 3.2. Stirring or exchange of water parcels can lead to change in the density of water parcels, and the associated vertical adjustment of the water column. The consequence of isopycnal stirring is examined in Section 3.3. As a result, the GPE of the system can be changed due to isopycnal stirring, as explained in Section 3.4. The GPE change due to subscale turbulent diffusion is examined in Section 3.5. Although isopycnal mixing has been discussed in many previous studies, some aspects of this problem have not been examined carefully. In Section 3.6, we will go through the energetics of stirring along arbitrary directions and show that stirring within a well-defined wedge is optimal in terms of GPE source/sink. The GPE release during isopycnal stirring can be connected with the elasticity, and this provides a close link between energetics of isopycnal stirring and water properties, as discussed in Section 3.7. Finally, this section is concluded in Section 3.8.

### 3.1 One cannot move a single parcel alone

Isopycnal eddy diffusion has been accepted as a classical concept. As our notion of isopycnal diffusion evolves, in some studies isopycnal diffusion is replaced by diffusion along Neutral Surface (NS). The NS has been defined as following: “Neutral surfaces are defined so that small isentropic and adiabatic displacements of a fluid parcel in a neutral surface do not produce a buoyancy restoring force on the parcel” (McDougall, 1987a); “A neutral trajectory is a three-dimensional path in the ocean, and is defined such that no buoyancy forces act on a water parcel when it is moved a small distance along this path” (Eden and Willebrand, 1999).

The exact meaning of NS was reexamined recently by Huang<sup>2)</sup>. A new terminology, the adiabatic density surface (ADS, denoted as  $\sigma_a$  hereafter), is introduced. This surface was previously discussed by McDougall (1987b), and it is defined as the depth at which the given water parcel can arrive through adiabatic movements, without changing its salinity and entropy.

The ADS associated with a water parcel at certain depth of a fixed station can be found as follows. Assume that a given water parcel moves adiabatically, without changing its potential temperature  $\Theta_0$  and salinity  $S_0$ . At time  $t$ , and at anywhere in the world oceans, its *in-situ* density is a function of the *in-situ* pres-

sure,  $\rho = \rho(\Theta_0, S_0, p, t)$ . On the other hand, taking a water column at any station  $(\lambda, \theta)$  in the world oceans, the *in-situ* density is a function of the *in-situ* pressure  $\rho = \rho[\Theta(\lambda, \theta, p, t), S(\lambda, \theta, p, t)]$ , where  $\Theta(\lambda, \theta, p, t)$ ,  $S(\lambda, \theta, p, t)$  are given functions at this station and need not equal to  $\Theta_0, S_0$ . For large-scale or meso-scale problems, the *in-situ* density monotonically increases with pressure. These two density functions constitute a nonlinear equation for a single unknown  $p$

$$\rho(\Theta_0, S_0, p) = \rho[\Theta(\lambda, \theta, p, t), S(\lambda, \theta, p, t), p]. \quad (13)$$

In general, there is a solution of this equation. Note that Eq. (13) may have multiple solutions, i.e., ADS can have multiple sheets/branches. Connecting these depths (pressures) in the world oceans gives the ADS. If this equation has no solution at a station, the ADS either outcrops or grounds.

Thus, for a water parcel taken at a given station and pressure level, the corresponding ADS is well defined through simple calculations. This family of surfaces is the only neutrally buoyant surface in the world oceans, and other surfaces different from this family of surface are not truly neutrally buoyant.

However, talking about the consequence of moving a single water parcel in the ocean may be physically incomplete. The ocean is a continuous media, so that one cannot talk about the consequence of moving a single parcel alone. Assume a water parcel A sitting at  $p=500$  ( $10^4$  Pa) leaves its original location and moves to a new location at  $p=1\,000$  ( $10^4$  Pa) on a potential density surface (PDS) (Fig. 12a). As a result, Parcel B originally at this location is repelled. In addition, there is an empty space left behind at  $p=500$  ( $10^4$  Pa), and other water parcels must come to fill up this space (Fig. 12b). A simple choice is to let Parcel B fill up this empty place (Fig. 12c), i.e. a position switch between these two parcels. Other choices must involve position exchange of multiple parcels. Thus, it is meaningless to talk about GPE change due to movement of a single parcel alone; instead, we must examine the total GPE change in the system due to movements of all relevant parcels.

The position exchange between Parcels A and B discussed here is of finite distance. If A and B are located on a NS or other

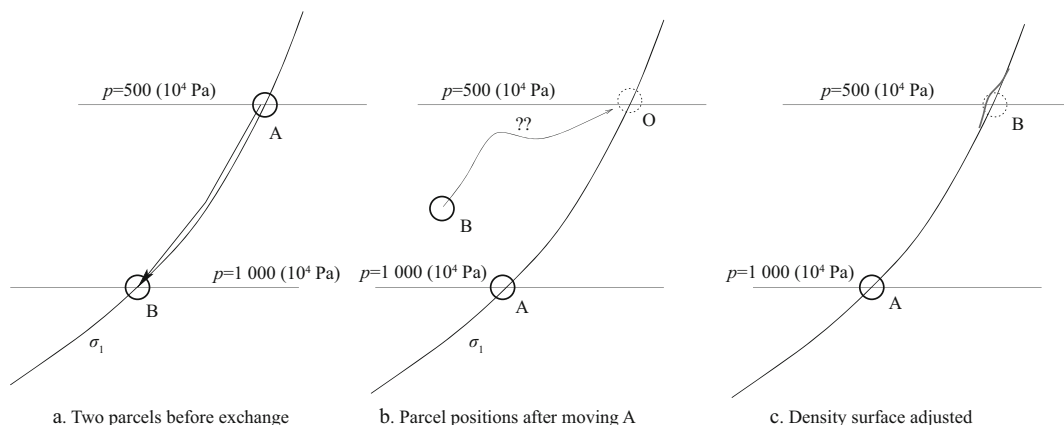


**Fig.12.** A sketch illustrating the consequence of moving a water parcel. The short solid curve in panel c indicates the possible distortion of the surface due to exchanging two water parcels on a PDS.

<sup>2)</sup> Huang R X. 2014. Adiabatic density surface, neutral density surface, potential density surface and mixing path. Manuscript submitted to Journal of Tropical Oceanography

types of density surface, one can also realize such an exchange through two series of infinitesimal position exchange as follows. First, we conceptually divide the water masses between parcels A and B into a series of parcels  $\{C_i\}$ ,  $i=1,2,3,\dots,N$ . Let Parcel A switch its position with  $\{C_i\}$ ,  $i=1,2,3,\dots,N$  on its left-hand side until it reaches the infinitesimal vicinity on the right-hand side of B. Second, let Parcel B switch its position with  $\{C_i\}$ ,  $i=N,\dots,3,2,1$ . At the end of these movements, A and B exchange their position without affecting any other parts of the system. If we assume that each position switch is infinitesimal, adiabatic and isentropic, the position exchanging of A and B also satisfies the basic assumption of adiabatic exchanges along a NS.

### 3.2 Thermobaric instability

We begin with examining an instability associated with thermohaline perturbations on PDSs. A typical case is the exchange of cold/fresh water from high latitudes and warm/salty water from mid-latitudes, depicted by the arrows in Fig. 13. The cold/fresh water from high latitudes is more compressible than the warm/salty water from middle latitudes. As will be shown shortly, this difference in elasticity can give rise to GPE release during isopycnal stirring of these two types of water. As a result, the quasi-lateral mesoscale intrusions between adjacent water masses on isopycnal surface can grow with energy supported by GPE released from the mean state through such exchanges, and this type of instability is called thermobaric instability.

Note that the instability discussed here is different from the thermohaline intrusion instability in connection with double diffusion. As discussed in many previous studies (Ruddick and Kerr, 2003; Ruddick and Richards, 2003), salt fingering and thermohaline intrusions appear on a vertical plane, such as  $(x, z)$  or  $(y, z)$ . Thus, these perturbations are examined in terms of fingering or layering in the vertical plane. Most importantly, the major mechanism driving such intrusions is directly linked to the differential diffusivity of temperature and salinity. Meanwhile, our discussion here is aimed at the isopycnal exchange of water parcels, and no difference in diffusivity of temperature and salt is involved in our analysis. Thus, although these two types of instability may be linked through some dynamical and thermodynamic processes, they are driven by quite different mechanisms and should have quite different characters.

### 3.3 Consequence of isopycnal stirring

In this section, we will show that isopycnal stirring is associated with GPE change of the system. The issue that isopycnal stirring is not energy free has been discussed in some of the early studies, such as McDougall (1987c) and Nycander (2011). The reader can find some of the relevant references in these two papers. However, we will examine this topic to a great details in this study.

We begin with two water parcels on the same PDS and exchange their right halves. Water Parcel 1 sits on pressure  $p_1=10^3$  ( $10^4$  Pa), so its *in-situ* density is equal to its potential density, i.e.  $\sigma_{1,1}=\sigma_{1,0}=\rho_{1,0}$ . Water Parcel 2 also sits on the same PDS, so that  $\sigma_{2,0}=\sigma_{1,0}$ ; however, it is on a slightly smaller pressure level  $p_2<10^3$  ( $10^4$  Pa), so its *in-situ* density satisfies  $\rho_{2,0}<\sigma_{1,0}$  (Fig. 14c).

When the right half of Parcel 2 moves to the position of the right half of Parcel 1, its new *in-situ* density is exactly equal to  $\sigma_{1,0}$ ; thus, GPE of water Column 1R remains unchanged. Due to the thermobaric effect, however, when the right half of Parcel 1 moves to the position of the right half of Parcel 2, its new *in-situ* density is different from that of the original water parcel. If the newly arrived water parcel has a density lower than the original *in-situ* density ( $\delta\rho_2=\rho_{2,1}-\rho_{2,0}<0$ ), the whole water column is pushed upward, and the sea surface is slightly higher (Fig. 14d). As a result, GPE of water Column 2R is increased. The slightly lower density in the right half of Parcel B induces a slightly upward distortion of the potential density, as indicated by the red curve in Fig. 12c. Therefore, although PDS consists of the same water parcels, the shape of the surface may change due to water parcel exchange. In addition, the cabbeling effect through subscale turbulent diffusion will increase the distortion of the surface further.

On the other hand, if the newly arrived water parcel has a density higher than the original *in-situ* density, the whole water column above should move downward, as shown in the right part of Fig. 14b; thus, GPE of water Column 2R is reduced, so that such water mass exchange is self-energized. Note that such self-energizing exchange of water mass is only in the sense of local energetics. In the global sense, the oceanic general circulation itself is incapable of generating mechanical energy, so that the local release of mechanical energy must be sustained by external mechanical energy source of global scale circulation.

### 3.4 GPE can change due to isopycnal stirring

All calculations in this section are based on the WOA01 data converted to the pressure coordinates (Conkright et al., 2002) described in Part I (Huang, 2014). As an example for isopycnal stirring, we examine water properties on  $\sigma_{0,5}=29.3$   $\text{kg/m}^3$  surface discussed in Part I (Huang, 2014). In particular, we plot the corresponding water properties along the 129.5°W meridional section in the North Pacific (Fig. 15). Along this section, both potential temperature and salinity decline with increasing latitude (Figs 15a and b); the bow-shaped subtropical gyre is clearly shown in the central part of Fig. 15c. In the northern part of this section, there is a clear sign of the dome-shaped subpolar gyre, indicated by the decline of depth (pressure of this potential density surface) with latitude. The most important feature is that elasticity increases with latitude, as both temperature and salinity decline (Fig. 15d).

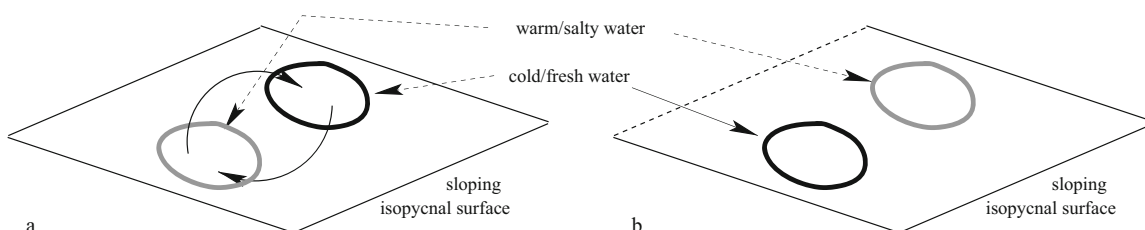


**Fig. 13.** A sketch of thermohaline intrusions through stirring on an isopycnal surface. a. Before stirring and b. after stirring.

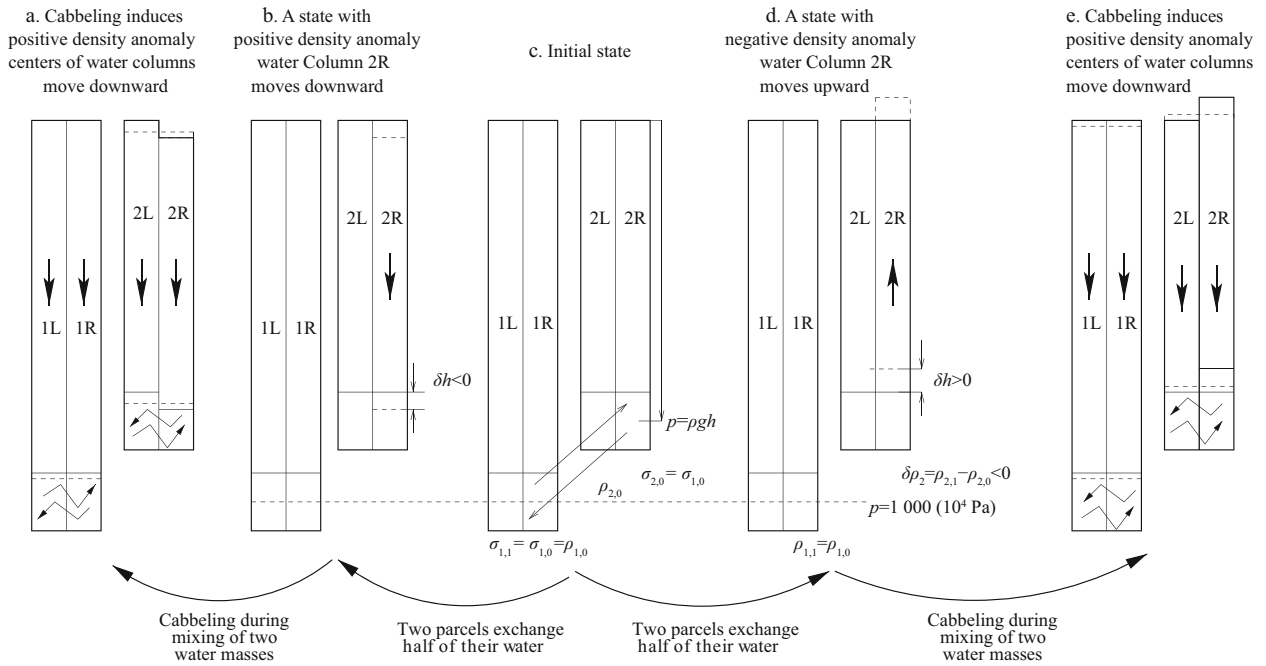


**Fig. 14.** A sketch illustrating the consequence of exchanging and mixing of two water parcels lying on the same PDS  $\sigma_1$ . Indexes 1L, 1R, 2L, 2R denote the left and right halves of the water Columns 1 and 2 respectively.

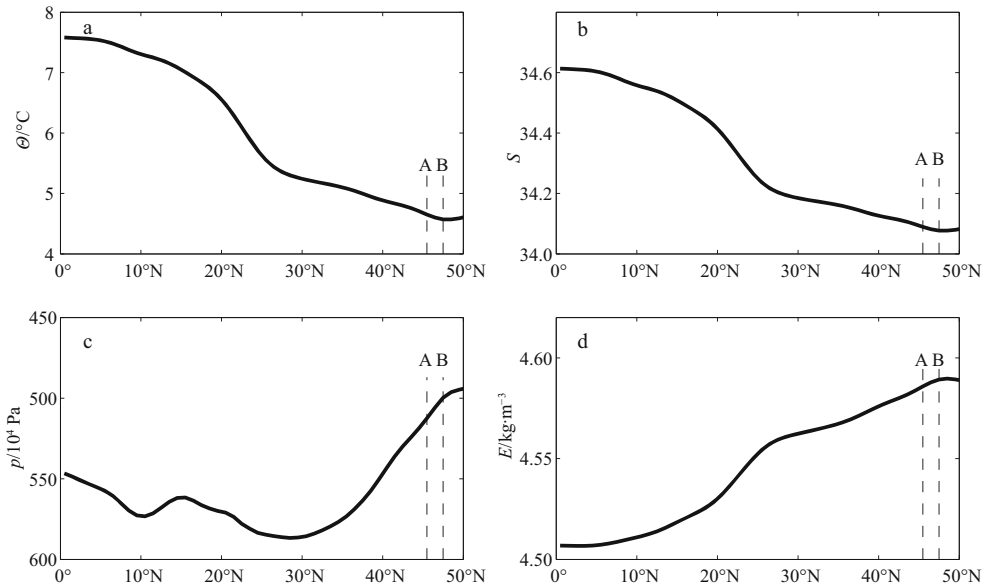


**Fig. 15.** Properties along the 129.5°W meridional section on PDS  $\sigma_{0,5}=29.3 \text{ kg/m}^3$ , including stations A and B. a. Potential temperature, b. salinity, c. depth and d. elasticity.

We now take two stations along this section, and the corresponding water properties are listed in Table 1. Elasticity at Station A is smaller than at Station B. Since at Station B the depth of PDS  $\sigma_{0,5}$  is very close to 500 ( $10^4 \text{ Pa}$ ), *in-situ* density is nearly equal to potential density, i.e.  $\sigma_t(B)=\sigma_{0,5}(B)=29.3 \text{ kg/m}^3$ .

By definition, when water Parcel A moves to Station B, its *in-situ* density  $\sigma_t(A \rightarrow B)$  should equal the *in-situ* density at B,

$\sigma_t(A \rightarrow B)=\sigma_t(B)=\sigma_{0,5}(B)=29.3 \text{ kg/m}^3$ . After exchanging their positions, the corresponding changes of *in-situ* density for Parcels A and B are

$$\Delta\sigma_{t,A} = \sigma_t(A \rightarrow B) - \sigma_t(A) = -E_A \Delta p, \quad (14a)$$

$$\Delta\sigma_{t,B} = \sigma_t(B \rightarrow A) - \sigma_t(B) = E_B \Delta p. \quad (14b)$$

**Table 1.** Basic properties at two stations taken from the 129.5°W meridional section of the PDS  $\sigma_{0.5}=29.3 \text{ kg/m}^3$ 

Station	$\theta/^\circ\text{C}$	S	$p/10^4 \text{ Pa}$	$E/\text{kg}\cdot\text{m}^{-3}$
A (45.5°N)	4.649 5	34.098	512.45	4.585 8
B (47.5°N)	4.571 7	34.077	499.75	4.589 2
Difference (B–A)	–0.037 8	–0.012	–12.70	0.003 4

The density difference is

$$\sigma_t(B \rightarrow A) - \sigma_t(A) = (E_B - E_A)\Delta p = 4.3 \times 10^{-5} (\text{kg/m}^3) > 0. \quad (15)$$

Therefore, when Parcel B arrives at Station A, its *in-situ* density is slightly higher than the original *in-situ* density of Parcel A. As a result, the whole water column above 512 ( $10^4 \text{ Pa}$ ) in Station A moves down and GPE is released. In addition, due to cabbeling more GPE is released after the incoming water mass is mixed with the local water mass. This release of GPE is an energy source sustaining the growth of isopycnal thermohaline intrusions.

The instability of quasi-horizontal thermohaline perturbations can be illustrated further by examining the GPE release associated with the meridional water mass exchange on this PDS. From Eq. (3), density change at Point C due to exchange between Points B and C along the PDS  $\sigma_{0.5}=29.3 \text{ kg/m}^3$  is

$$\Delta\rho_{B \rightarrow C} = (E_B - E_C)\Delta p_{B \rightarrow C}. \quad (16)$$

Change in the water parcel's height is  $\delta h = -\delta\rho\Delta h / \bar{\rho}$ , where  $\bar{\rho}$  is the mean reference density. Thus, the change in GPE for the water column above Point C is

$$\Delta\chi_{B \rightarrow C} = p_C\delta h = -p_C\Delta h\delta\rho_{B \rightarrow C} / \bar{\rho} = -p_C\Delta h(E_B - E_C)\Delta p_{B \rightarrow C} / \bar{\rho}. \quad (17)$$

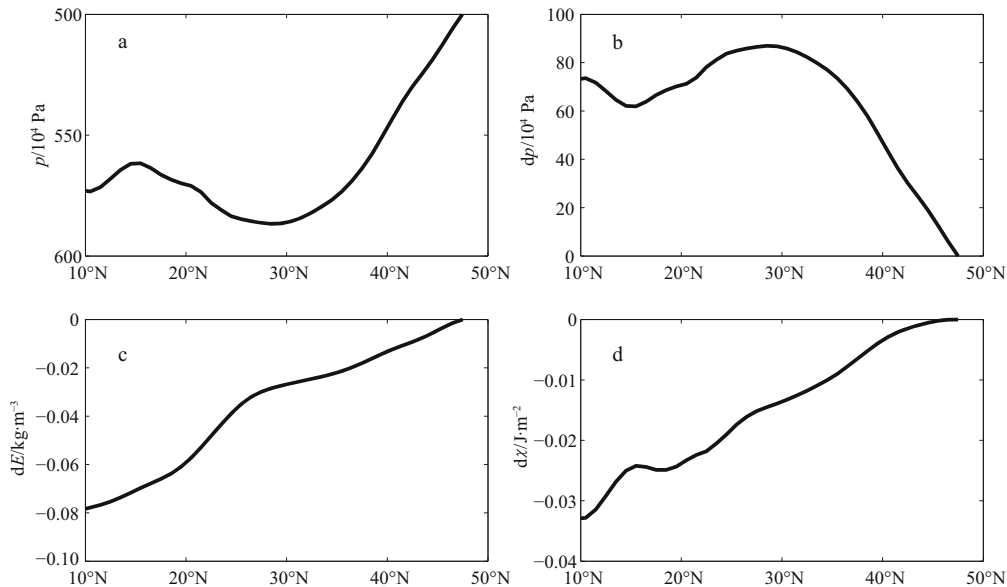
Assuming the water parcel height is  $\Delta h=1\text{m}$ , the change in GPE due to exchanging water parcels along a section through 129.5°W is shown in Fig. 16. Since pressure along this section varies only slightly between 500 and 580 ( $10^4 \text{ Pa}$ ), the change in GPE is proportional to the difference in pressure and elasticity. In the vicinity of Point B, these two terms are almost linearly proportional to the distance from Point B; thus, the GPE release (sink) is proportional to the square of the distance from Point B. In the far field, the energy sink gradually turns into a linear function of the distance (Fig. 16d).

The most important point from this calculation is that lateral exchange of water masses on the PDS can lead to GPE released from the mean state. Thus, such thermohaline perturbations are self-energized.

### 3.5 GPE change associated with subscale turbulent diffusion

During the second stage, the left and right halves of water Column 1 and 2 are mixed. Due to the cabbeling effect, the density of the mixed product is higher than the mean density of the parent water masses. As a result, the whole water column and the mean sea level move downward (Figs 14a and e). In general, cabbeling always releases GPE, and it is self-energized. Of course, the mechanical energy released associated with cabbeling must come from some of the external sources of mechanic energy for the global ocean circulation.

The net GPE change due to isopycnal diffusion is the sum of these two processes. If the net GPE change is negative, the isopycnal diffusion is self-energized. On the other hand, if


**Fig. 16.** Energy released through meridional mass exchange between Station B (47.5°N) and a station south along the 129.5°W section on PDS  $\sigma_{0.5}=29.3 \text{ kg/m}^3$ .

the net GPE change is positive, isopycnal diffusion cannot be self-sustained, and some local sources of mechanical energy is required. Since cabbeling associated with subscale diffusion always leads to release of GPE, our analysis in this section is focused on the GPE change due to isopycnal stirring associated with isopycnal eddy diffusion.

### 3.6 GPE change associated with isopycnal stirring

#### 3.6.1 Stirring along different directions in space

Isopycnal diffusion has been accepted as a common knowledge. The reason of why lateral diffusion has to take place along isopycnal has not been examined thoroughly. Is there some other directions which is even better for lateral diffusion?

To answer this question, we first examine the exchange of two parcels along the intersection ( $\vec{s}$ , red line with arrow, Fig. 17) between a pressure surface  $P$  (green) and a PDS  $\sigma_p$  (black, using reference pressure  $p$ ). Although these two parcels have different temperature and salinity, they have the same *in-situ* density under pressure  $p$ . Since they sit on the same pressure surface, exchanging these two parcels does not change density; thus, stirring along line  $\vec{s}$  does not alter the GPE of the system.

On the other hand, due to cabbeling effect when these two parcels mix with the local water, the density of the mixture is higher than the original parcels. Therefore, the total volume of the water parcels shrink, the corresponding centers of water columns above these parcels move downward. As a result, GPE is released. However, in this section our discussion is focused on the consequence of stirring alone; thus, we will not discuss the consequence of cabbeling due to the subscale diffusion.

Our next step is to examine the consequence of stirring along all possible directions in the three dimensional space. As shown in Fig. 17, stirring can be project to two components: stirring along vector  $\vec{s}$  and on the blue plane  $V$  perpendicular to it. Since stirring along  $\vec{s}$  does not change GPE, we will examine what happens if parcels are exchanged in all potential directions on the plane  $V$  (blue) perpendicular to the vector  $\vec{s}$  in Fig. 17. On this plane, we can identify four vectors: the “horizontal” (constant pressure) vector  $\vec{h}$ , the normal vector  $\vec{N}$  of the PDS  $\sigma_p$ , a vector  $\vec{n}$  which is on the PDS and perpendicular to both vectors  $\vec{s}$  and  $\vec{N}$ . In addition, there is a vector  $\vec{z}$  which is opposite to the direction of gravitational force.

It is well known that diffusion along the direction of  $\vec{N}$  or  $\vec{z}$  requires doing work against gravitational force. We discussed the GPE change due to vertical stirring, i.e. along  $\vec{z}$ , in Section 1. Vector  $\vec{n}$  is on the PDS, so isopycnal stirring and subscale diffusion should take place along this direction; thus, our focus here is to examine what happens in the vicinity of vector  $\vec{n}$ . We will take a plane view looking from the left side to right side of Fig. 17.

#### 3.6.2 Wedge of maximum GPE release

The first example is a meridional section through station (48.5°S, 30.5°W). The pivotal PDS is  $\sigma_1$ , the horizontal line passing Point O is at constant pressure  $p=1\,000$  ( $10^4$  Pa), the vertical axis is in pressure coordinate (Fig. 18). This station is within the strong front of ACC, so that this PDS slopes up southward. At Station S, 1° south of Station O, the  $\sigma_1$  surface intersects at a depth of 877.020 ( $10^4$  Pa); the constant *in-situ* density surface  $\sigma$  intersects at depth of 989.4 ( $10^4$  Pa); the ADS  $\sigma_a$  intersects at depth of  $p_p=877.407$  ( $10^4$  Pa). By definition, water parcel from

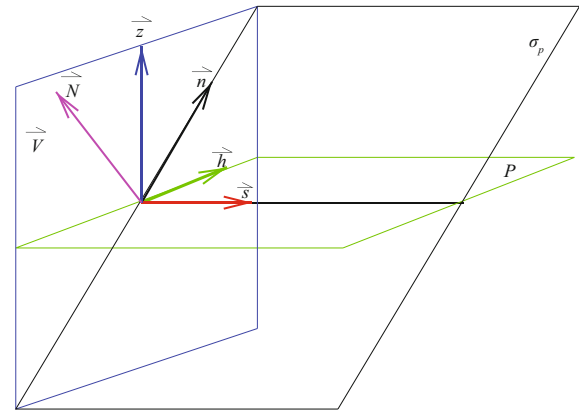


**Fig. 17.** A sketch of the basic vectors on the pressure surface (green), PDS (black) and the plane (blue) perpendicular to these two surfaces.

Point O should arrive at pressure  $p_p=877.407$  ( $10^4$  Pa) level in Station S adiabatically and acquires the local *in-situ* density. In fact,  $\sigma_a$  is the PDS starting from  $p_p$  at Station S and intersects Station O at 1 000 ( $10^4$  Pa) level. Thus,  $\sigma_1$  and  $\sigma_a$  are two PDSs passing through Point O. As will be shown, the wedge defined by these two special PDSs is an optimal edge of isopycnal stirring.

Density and its anomaly due to parcel exchanges are shown in Fig. 18b. Density of two water parcels originating from Point O and Station S are denoted as follows: Parcel O originally locates at Point O, and Parcel UL originally locates at the upper or upper left of Parcel O. The distance of color curves from origin O schematically indicates density of these water parcels, as a function of the angle  $\theta$ . Here again, the angle  $\theta$  shows the angle distance from horizontal ( $\theta=0^\circ$ ) to vertical ( $\theta=90^\circ$ ). Note that in this figure the vertical distance along the vertical axis and the angle distance is not the accurate distance, and they are used for schematically illustration only.

Starting from line OU, Parcel UL lies above Parcel O. For large-scale circulation the stratification is stable. Hence, Parcel O is heavier than Parcel UL, as shown by the intersection of thin blue and red line with the vertical line OU in Fig. 18b. If we exchange their positions, density of Parcel O declines during its upward motion,  $\rho(O \rightarrow UL) < \rho(O)$ , i.e. the heavy red curve is below the thin blue curve. However, when Parcel O arrives at the original location of Parcel UL, the corresponding density anomaly is positive, i.e.  $\rho(O \rightarrow UL) > \rho(UL)$ . On the other hand, due to compression density of Parcel UL increases, and it satisfies  $\rho(UL) < \rho(UL \rightarrow O) < \rho(O \rightarrow UL)$ , as shown in Fig. 18b.

If the newly arriving parcel has a density lower (higher) than the *in-situ* density of the original parcel at the same location, water column above is pushed upward (downward) and GPE is increased (reduced), and external source of mechanical energy is required (released). As we turn the angle anticlockwise, the amplitude of density anomaly declines (Fig. 18b). PDS  $\sigma_1$  intersecting the water column at Station S at Point A,  $p=877.020$  ( $10^4$  Pa), is a critical boundary of the domain discussed above (Fig. 18a). By definition, a parcel moving from Point A to the origin O should have the same *in-situ* density at Point O, i.e.  $\rho(UL \rightarrow O) < \rho(O)$  and the two blue curves intersect (Fig. 18b).

After the exchange, however, the *in-situ* density of Par-

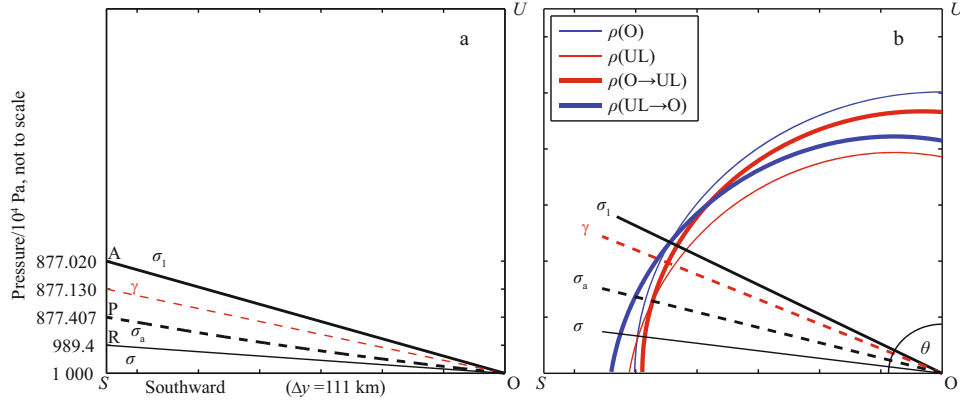


**Fig. 18.** A sketch of potential density line  $\sigma_1$ , adiabatic density line  $\sigma_a$  and neutral line  $\gamma$  (a. density surfaces in a meridional section); density at the new location after exchange, as compared with the local *in-situ* density (b.  $\rho$  and  $\rho_{in-situ}$  as a function of the angle). Calculations are based on a meridional section along 30.5°W at 49.5°S and 48.5°S.

cel O is larger than that of the parcel originally at Point A, i.e.  $\rho(O \rightarrow UL) > \rho(UL)$ , so the heavy red curve is outside the thin red curve. Thus, if these two parcels on this PDS exchange their positions, the water column above Point A shrinks and the total GPE will be reduced, so that such a water mass exchange is self-energized.

As we turn the angle further anticlockwise,  $\rho(UL \rightarrow O) - \rho(O)$  becomes positive, but  $\rho(O \rightarrow UL) - \rho(UL)$  continues to decline. The ADS  $\sigma_a$  is the second critical boundary. At Station S, it intersects at  $p = 877.407$  ( $10^4$  Pa) (point P in Fig. 18a). By definition, it satisfies  $\rho(O \rightarrow UL) = \rho(UL)$ ; however,  $\rho(UL \rightarrow O) > \rho(O)$ , i.e. the *in-situ* density of water Parcel UL at Point O is larger than the original *in-situ* density there, as shown in Fig. 18b and Table 2. Therefore, the water column at Station O should move downward and GPE will be released. Hence, within the wedge between  $\sigma_1$  and  $\sigma_a$  water parcel exchange leads to the release of GPE and such exchange is self-energized. In addition, cabbeling should lead to more GPE released.

If we continue to rotate the angle anticlockwise,  $\rho(O \rightarrow UL)$  becomes smaller than  $\rho(UL)$ ; this implies that external mechanical energy is needed for supporting the increase of GPE. Although there is energy released due to water column shrinking associated with moving the water parcel from the upper left to Point O, such energy is mostly lost through turbulence and dissipation. Thus, water mass exchange along such an angle cannot be self-sustained.

Near the end of rotation is the *in-situ* density surface (thin solid black lines in Fig. 18). Although  $\rho(O \rightarrow UL) < \rho(UL)$ , i.e. GPE at Station S is released, it is mostly dissipated through turbulence. On the other hand, a further increase in  $\rho(UL \rightarrow O) - \rho(O)$

suggests that GPE at Station O is increased, hence more energy is required for sustaining exchange along this line.

The end of this rotation is exchanging along the constant pressure  $p = 1000$  ( $10^4$  Pa). The corresponding density anomalies are quite large (Fig. 18b). This figure clearly suggests that GPE change associated with horizontal stirring is much larger than isopycnal stirring.

The discussion above is based on information at two separate stations only, and the PDS is represented by two points at these two stations. We can increase the resolution by dividing the distance between Stations O and S into many sub-stations with horizontal grids with resolution of  $(1/10)^\circ$ ,  $(1/100)^\circ$ , and  $(1/1000)^\circ$ . Temperature and salinity at these refined grid points are calculated by linear interpolation from the  $1^\circ$  grid. A neutral line can be found by following the original idea of Forster and Carmack (1976), using the simple Euler forward method. Starting from Point O, one can find the intersection of the  $\sigma_1$  PDS with the next sub-station on its southern side. Denote the corresponding depth (pressure) of this intersection as  $p_1$ , then a new PDS  $\sigma_{p_1}$  can be defined, and its intersection with the next station on the left side can be found. In this way, a neutral line  $\gamma$  between Stations O and S can be calculated step by step.

On the other hand, both the potential density lines and adiabatic density lines are independent of the resolution used in calculation because the depth of these surfaces at any given station is defined completely independent of the water mass properties in the adjacent stations. Depth differences between potential density lines  $\sigma_1$  and adiabatic density lines  $\sigma_a$  or neutral lines  $\gamma$  for different horizontal resolutions between Station O and S are shown in Fig. 19.

**Table 2.** Density and its perturbations at three critical boundaries for the meridional section shown in Fig. 18

Point	$p/10^4$ Pa	$\sigma_p$	$\sigma_1(O) - \sigma(p)$	$\sigma_1(p) - \sigma_1(O)$	$\sigma_p(O) - \sigma_p(p)$
A	877.0202	31.72230	0.5663	0.000000	0.0001663
P	877.4066	31.72430	0.5645	0.0001669	0.000000
R	989.4128	32.23904	0.0000	0.0487180	-0.0486720

Notes: Density in  $\sigma$  unit ( $\text{kg/m}^3$ ).  $p$  indicates local pressure, and it is also used to denote the water parcel taken from Station S at local pressure  $p$ ;  $\sigma_p$  is the potential density using the local pressure  $p$  as the reference pressure,  $\sigma(p)$  is the *in-situ* density at local pressure  $p$ ;  $\sigma_1(O) = \sigma_1^0$  and  $\sigma_p(O)$  indicate potential density of water Parcel O at reference pressure 1000 ( $10^4$  Pa) and  $p$ ;  $\sigma_1(p)$  and  $\sigma_p(p)$  indicate potential density of water parcel  $p$  at reference pressure 1000 ( $10^4$  Pa) and  $p$ .

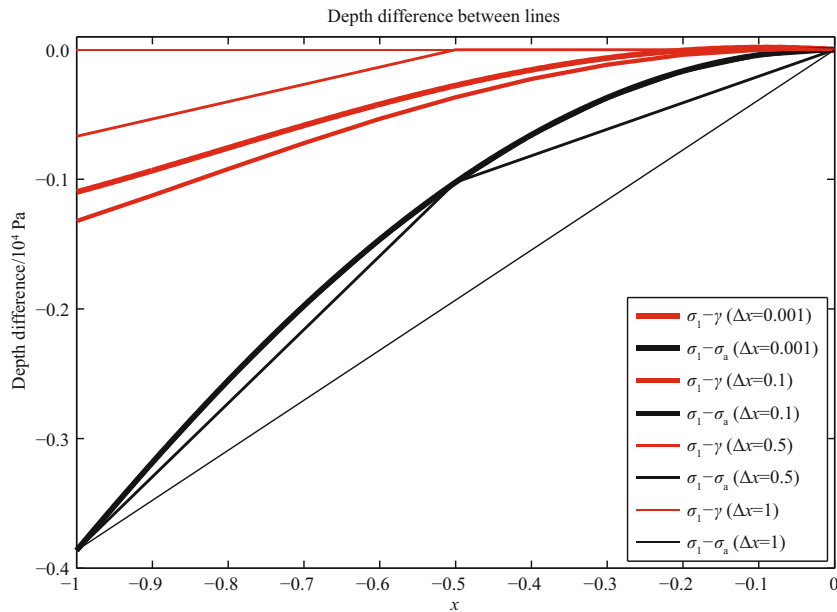


**Fig.19.** Depth difference between the potential surface line with adiabatic density line and neutral lines constructed by different horizontal resolutions for the station based on a meridional section along 30.5°W at 49.5°S and 48.5°S. Note that  $\sigma_1 - \sigma_a$  are nearly identical for resolution of 0.1 and 0.001; thus, these two curves cannot be seen separately in this figure.

By definition, for the case with a single step from Station O to S, the neutral line  $\gamma$  is coincident with that of a potential density line  $\sigma_1$ ; but  $\sigma_a$  is different from  $\sigma_1$ . As the horizontal resolution is increased, the end point of the  $\gamma$  line varies slightly because the solution is resolution dependent. For resolution of 0.001 or higher, the neutral line converges to its limiting shape. The limit shape of the neutral line is schematically shown in Fig. 18 as the red lines. For the present case, its position is within the subscale turbulent diffusion wedge, i.e., between  $\sigma_1$  and  $\sigma_a$ . As shown above, the wedge of maximum GPE release is independent of the grid resolution.

The exact information of density perturbation induced by water mass exchange is shown in Fig. 20. As discussed above, negative (positive) density perturbation indicates that the corresponding water column above must be push upward (downward), i.e. such an exchange needs (releases) mechanical energy.

As shown in Fig. 20b, when the water parcel from the upper left moves to Point O, the density anomaly at Point O is gradually increased from a large negative value. At the intersection of  $\sigma_1$ , density anomaly at Point O is exactly zero, as required by the definition of PDS. At this point, density anomaly at Point A is still positive.

We now select water Parcel UL level at Station S at a deeper level. At the intersection of  $\sigma_a$ , density anomaly at Point A is exactly zero, but density anomaly at Point O has a small positive value. Therefore, the wedge defined by these two surfaces is the region where the density anomaly induced by exchange is non-negative. As a result, such exchange must induce the release of GPE, and thus it is self-energized.

As indicated by the solid red line in Fig. 20b, the sum of density anomaly at these two stations is practically constant within this wedge. The amount of GPE released due to the water parcel exchange is the product of density anomaly and the *in-situ*

pressure. If we neglect the small difference in pressure at these two points, the total amount of GPE released due to water mass exchange is constant within this wedge.

Above this wedge, the GPE release at Station S is larger than the value indicated by the red line. However, the GPE change at Station O becomes negative; thus, external mechanical energy is needed. Since GPE released at Station S is mostly lost to small scale turbulence, exchange above the wedge may require external mechanical energy for support, so it is less likely to happen. The situation below the wedge is quite similar.

We have thus modified the classical conception of isopycnal stirring: instead of claiming that water parcels can move along isopycnal surfaces (or NSs) free of GPE change, we state that isopycnal surfaces within the optimal wedge are the most favorable surfaces for lateral stirring.

### 3.6.3 Wedge of minimum GPE source

As the second example, we discuss the situation at another station (20.5°N, 149.5°E) (Fig. 21a). The situation is similar to Fig. 18. However,  $\sigma_1$  intersects the water column at Station S south of station O at a pressure lower than  $\sigma_a$  (Fig. 10a); thus, density anomalies on these two boundaries are opposite to the case in Fig. 18b.

By definition, when Parcel O moved to the upper left part along the  $\sigma_a$  surface, it should have the same density as the local water parcel, indicated by the intersection between the thin and red curves with the dashed black line in Fig. 21b. However, the water parcel moved from the upper left part to Point O has a density (heavy blue curve) smaller than the local density (thin blue curve) (Fig. 21b). As we continue to rotate the angle and reach PDS  $\sigma_1$ ,  $\rho(O \rightarrow UL) - \rho(UL)$  becomes negative. By definition, the parcel that moved along  $\sigma_1$  from the upper left part to Point O has the same density as the original local parcel. Thus, within the wedge defined by  $\sigma_a$  and  $\sigma_1$  water parcel exchange will lead

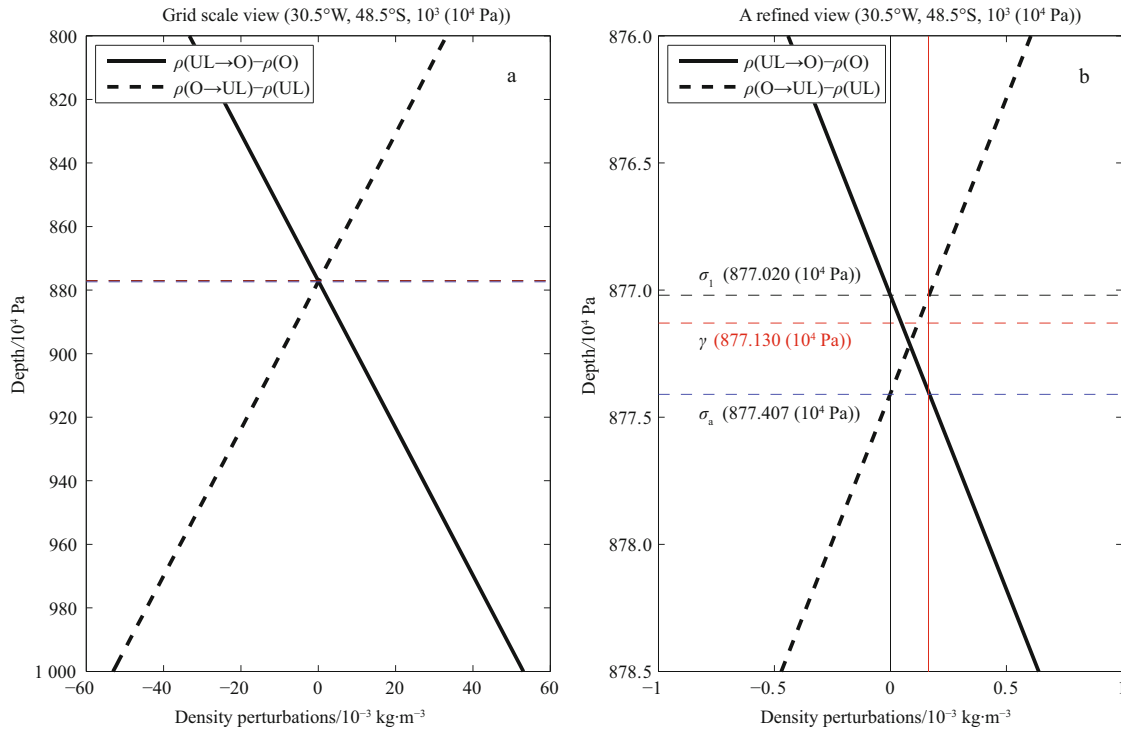


**Fig.20.** Density perturbations obtained by exchanging water parcels O and UL, based on a meridional section along 30.5°W at 49.5°S and 48.5°S; the vertical axis indicates the pressure level where parcel UL is originally located. The red line in panel b indicates the sum of density anomaly of these two water parcels.

to a negative density anomaly; thus, this leads to a source of GPE, and external mechanical energy is required for sustaining this exchange. The corresponding neutral line  $\gamma$  with resolution of  $\Delta x=0.001^\circ$  is schematically shown as the dashed red lines in Fig. 21. The corresponding density perturbations induced by exchanging water parcels are listed in Table 3.

Density perturbations induced by water mass exchange are shown in Fig. 22. Negative density perturbation indicates that external mechanical energy is needed; while positive density perturbation implies release of GPE, and the exchange is self-energized. Here again, a refining neutral line seems to be locat-

ed within the wedge defined by  $\sigma_a$  and  $\sigma_1$ .

The red vertical line in Fig. 22b indicates the sum of density anomaly at these two stations. Hence,  $\sigma_a$  and  $\sigma_1$  define a wedge, in which density anomalies associated with both water parcels are negative, and their sum is constant. If we neglect the small difference in pressure at these two points, the total GPE increase due to parcel exchange is constant within this wedge.

Above this wedge, density anomaly at Station O becomes more negative, implying that more external mechanical energy is need for supporting the exchange. Although density anomaly at Station S becomes positive, GPE released is mostly dissipated

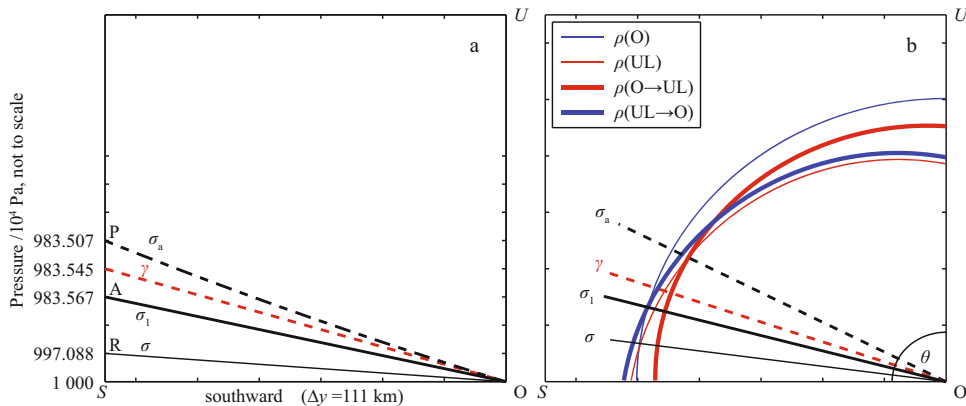


**Fig.21.** A sketch of PDSs (a. density surfaces in a meridional section); density at the new location after exchange, as compared with the local *in-situ* density (b.  $\rho$  and  $\rho_{in-situ}$  as a function of the angle), based on a meridional section along 149.5°E at 19.5°N and 20.5°N.

**Table 3.** Density and its perturbations at three critical boundaries for the meridional section presented in Fig. 21

Point	$p/10^4$ Pa	$\sigma_p$	$\sigma_1(O)-\sigma(p)$	$\sigma_1(p)-\sigma_1(O)$	$\sigma_p(O)-\sigma_p(p)$
P	983.507 2	31.871 60	0.075 000	-0.000 058	0.000 000
A	983.566 5	31.871 90	0.074 800	0.000 000	-0.000 058
R	997.088 0	31.932 69	0.000 000	0.013 249	-0.012 335

**Note:** Density in  $\sigma$  unit ( $\text{kg}/\text{m}^3$ ).  $p$  indicates local pressure, and it is also used to denote the water parcel taken from Station S at local pressure  $p$ ,  $\sigma_p$  is the potential density using the local pressure  $p$  as the reference pressure,  $\sigma(p)$  is the *in-situ* density at local pressure  $p$ ;  $\sigma_1(O)=\sigma_1^0$  and  $\sigma_p(O)$  indicate potential density of water Parcel O at reference pressure 1 000 ( $10^4$  Pa) and  $p$ ;  $\sigma_1(p)$  and  $\sigma_p(p)$  indicate potential density of water parcel  $p$  at reference pressure 1 000 ( $10^4$  Pa) and  $p$ .

through small scale processes. Hence, exchange in the domain above the wedge should require more external mechanical energy for support. The situation below the wedge is similar. Therefore, we conclude that stirring within this wedge requires the least amount of external mechanical energy. Hence, this wedge can be called the edge of minimum GPE source.

### 3.7 GPE change in terms of elasticity

The density anomaly discussed above can be more conveniently calculated in terms of elasticity. As shown in Fig. 21, for small isentropic and isohaline perturbations we have

$$\begin{aligned}\rho(O \rightarrow A) &= \rho(O) + \rho_0 K_\eta (S_O, \Theta_O, \bar{p}) \delta p \\ &= \rho(O) + E(S_O, \Theta_O, \bar{p}) \delta p / 1\,000,\end{aligned}\quad (18a)$$

$$\begin{aligned}\rho(A \rightarrow O) &= \rho(A) - \rho_0 K_\eta (S_A, \Theta_A, \bar{p}) \delta p \\ &= \rho(A) - E(S_A, \Theta_A, \bar{p}) \delta p / 1\,000,\end{aligned}\quad (18b)$$

where  $E$  is elasticity,  $\bar{p}=0.5(p_O+p_A)$  is the mean pressure of these two points, and  $\delta p=p_A-p_O=-16.433$  ( $10^4$  Pa) $<0$ . Since  $\rho(O)=\rho(A \rightarrow O)$ , Eqs (18a) and (18b) lead to

$$\begin{aligned}\rho(O \rightarrow A) - \rho(A) &= -[E(S_A, \Theta_A, \bar{p}) - E(S_O, \Theta_O, \bar{p})] \delta p / 1\,000 \\ &= -\delta E \delta p / 1\,000 < 0.\end{aligned}\quad (19)$$

One may use the elasticity based on the local pressure

$$\begin{aligned}\delta \rho^* &= -[E(S_A, \Theta_A, p_A) - E(S_O, \Theta_O, p_O)] \delta p / 1\,000 \\ &= -\delta E^* \delta p / 1\,000.\end{aligned}\quad (20)$$

However, Eq. (20) is less accurate because these two values of elasticity are calculated at a different pressure (Table 4). If the same reference pressure, either the pressure at Point O or the middle point between these two points, is used in calculating the elasticity difference, the result is very close to that calculated directly from the density difference as discussed above.

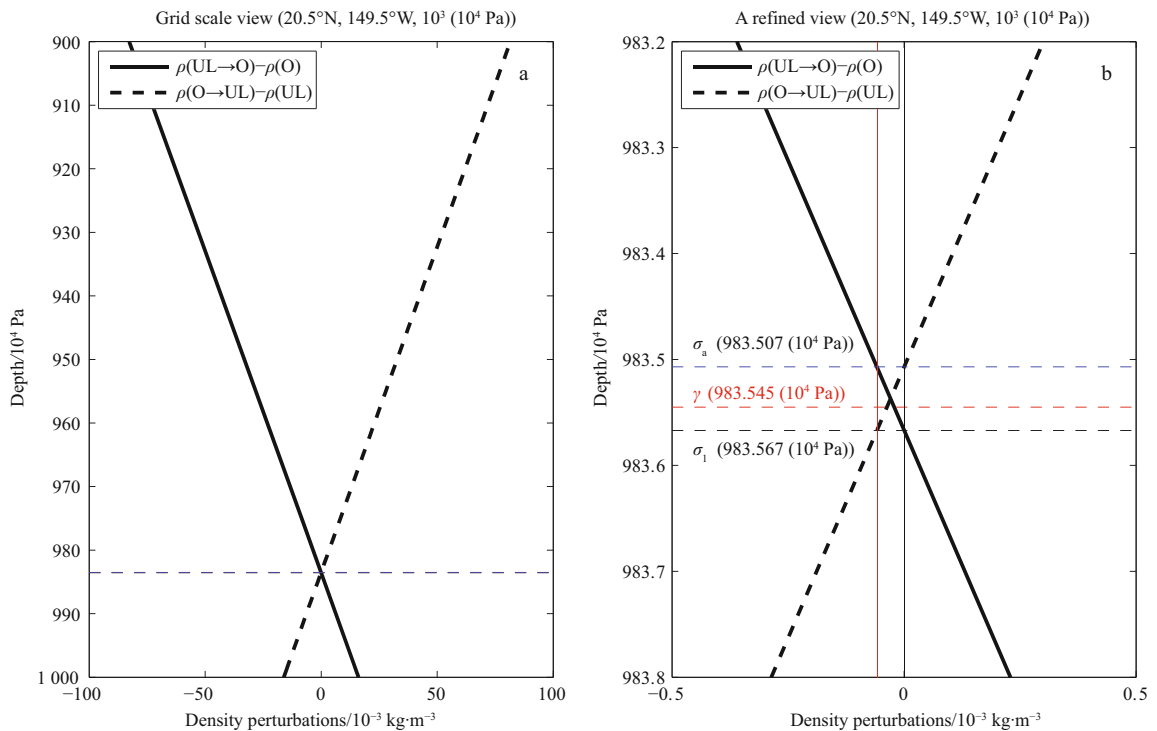


**Fig.22.** Density perturbations obtained by following PDS defined in different ways, based on a meridional section along 149.5°W at 20.5° and 19.5°N.

The analysis above is based on pressures at the Stations O and S. From Figs 18b and 21b, it is convenient to use the mean pressure between these two stations, and the density anomaly at Stations O and S should be equal to half of the density anomaly displayed in Figs 20b and 22b.

Assume there are two parcels, Parcels B and T, on the same PDS  $\sigma_o = \rho_{00}$  (Fig. 23). The pressure difference between these two water parcels is  $\Delta p = p_B - p_T > 0$ . The mid pressure level is  $p_O = (p_T + p_B) / 2$ . Denote *in-situ* density of water Parcel B and Locations B, O, and T as  $\rho(B)$ ,  $\rho(B \rightarrow O)$ ,  $\rho(B \rightarrow T)$ , and *in-situ* density of water parcel T and locations T, O, and B as  $\rho(T)$ ,  $\rho(T \rightarrow O)$ ,  $\rho(T \rightarrow B)$ . When water Parcels B and T move to pressure level  $p_O$ , their *in-situ* density match the *in-situ* density of the water parcel originally sitting there, i.e.

$$\rho(B \rightarrow O) = \rho_{00} = \rho(T \rightarrow O). \quad (21)$$

Thus, the *in-situ* density of these parcels can be written as follows

$$\begin{aligned} \rho(B) &= \rho_{00} + E(B, O) \Delta p / 2000, \\ \rho(B \rightarrow T) &= \rho_{00} - E(B, O) \Delta p / 2000, \end{aligned} \quad (22)$$

$$\begin{aligned} \rho(T) &= \rho_{00} - E(T, O) \Delta p / 2000, \\ \rho(T \rightarrow B) &= \rho_{00} + E(T, O) \Delta p / 2000, \end{aligned} \quad (23)$$

where  $E(B, O)$  and  $E(T, O)$  are the elasticity of water Parcels B and T at Point O. Hence, after exchange the *in-situ* density anomalies at Stations B and T are

$$\rho(T \rightarrow B) - \rho(B) = [E(T, O) - E(B, O)] \Delta p / 2000, \quad (24)$$

$$\rho(B \rightarrow T) - \rho(T) = [E(T, O) - E(B, O)] \Delta p / 2000. \quad (25)$$

In this way, during isopycnal stirring density anomalies at both stations are the same. Eq. (19) can be rewritten as follows

$$\begin{aligned} \delta\rho &= \rho(O \rightarrow A) - \rho(A) \\ &= -[E(S_A, \Theta_A, p_O) - E(S_O, \Theta_O, p_O)] \delta p / 1000 \\ &= -\left[ \frac{\partial E}{\partial \Theta} \frac{\partial \Theta}{\partial p} \Big|_{\bar{n}} + \frac{\partial E}{\partial S} \frac{\partial S}{\partial p} \Big|_{\bar{n}} + \frac{\partial E}{\partial p} \Big|_{\bar{n}} \right] \delta p^2 / 1000. \end{aligned} \quad (26)$$

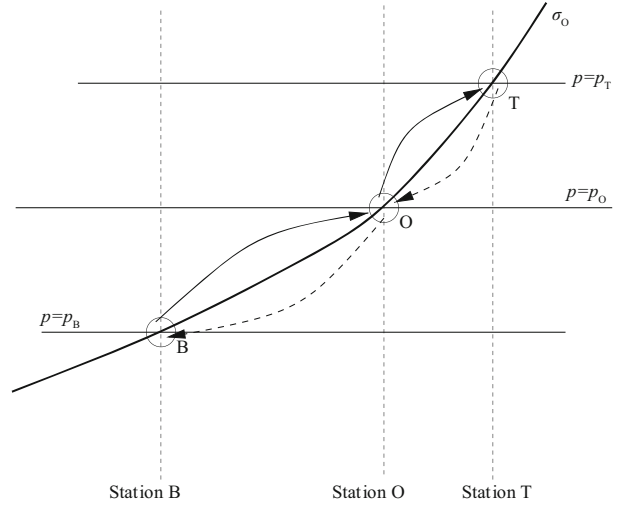


**Fig. 23.** A sketch illustrating exchanging of two water parcels lying on the same PDS  $\sigma_o$  and with equal pressure difference above and below the reference pressure  $p_o$ .

where  $\delta\theta = \theta_A - \theta_O$ ,  $\delta S = S_A - S_O$ , and  $\bar{n}$  is the normal vector shown in Fig. 17. The corresponding change of the layer thickness is  $\delta h = -\Delta h \delta\rho / \rho_0 > 0$ . The water column above pressure level  $p_s$  is pushed upward, and the increase of GPE of the system is

$$\delta\chi = p\delta h A_s = -p\Delta h A_s \delta\rho / \rho_0 = \frac{p\Delta h A_s}{1000\rho_0} E_i \delta l^2, \quad (27)$$

where

$$E_i = \left[ \frac{\partial E}{\partial \Theta} \frac{\partial \Theta}{\partial l} \Big|_{\bar{n}} + \frac{\partial E}{\partial S} \frac{\partial S}{\partial l} \Big|_{\bar{n}} + \frac{\partial E}{\partial p} \frac{\partial p}{\partial l} \Big|_{\bar{n}} \right] \frac{\partial p}{\partial l} \Big|_{\bar{n}} = \nabla E \cdot \nabla p, \quad (28)$$

and  $\delta l$  is the horizontal grid size, or the distance between centers of these two water parcels. Wherever  $\nabla E \cdot \nabla p < 0$ , GPE is reduced due to isopycnal stirring; thus, perturbations are self-energized. On the other hand,  $\nabla E \cdot \nabla p > 0$ , external source of mechanical energy is needed for sustaining isopycnal stirring. In general, the first term in Eq. (28) dominates. Since  $\partial E / \partial \theta < 0$ , when potential temperature increases with increase of pressure,  $E_i < 0$  is satisfied.

As an example, the horizontal distribution of the  $\nabla E \cdot \nabla p$  term on the  $\sigma_{0.5} = 29.3 \text{ kg/m}^3$  PDS is shown in Figs 24 and 25. Because the magnitude of negative values is 100 times larger than the positive values, we show the maps of negative and positive

**Table 4.** Changes in density, pressure level, and elasticity for two stations shown in Figs 18 and 21

Station position	$p / 10^4 \text{ Pa}$	$\delta p / 10^{-3} \text{ kg}\cdot\text{m}^{-3}$	$\delta p / 10^4 \text{ Pa}$	Using the same reference pressure		Using local (different) reference pressures	
				$\delta E$	$\delta\rho = \frac{\delta E \delta p}{1000}$	$\delta E^*$	$\delta\rho^* = \frac{\delta E^* \delta p}{1000}$
49.5°S, 30.5°W	877.0	0.1663	-123.0	0.001353	0.16630	0.001430	0.17590
20.5°N, 149.5°E	983.6	-0.0580	-16.4	-0.003526	-0.05793	-0.001819	-0.02988

Notes: Unit of  $\delta E$  is  $\text{kg/m}^3$ , unit of  $\delta\rho = \frac{\delta E \delta p}{1000}$  is  $10^{-3} \text{ kg/m}^3$ , unit of  $\delta E^*$  is  $\text{kg/m}^3$ , unit of  $\delta\rho^* = \frac{\delta E^* \delta p}{1000}$  is  $10^{-3} \text{ kg/m}^3$ .

values separately. From Fig. 24, it is clear that the band of the ACC and the Gulf Stream are the places associated with a large amount GPE release associated with isopycnal diffusion.

Since the isopycnal surface and other properties have strong meridional gradient, the related thermobaric instability discussed here tends to intensify in certain direction. Thus, isopycnal diffusion supported by external source of mechanical energy should be non-isotropic in nature. However, this issue is left for further study.

On the other hand, in the equatorward edge of the subtropical gyres in the Pacific, the meridional pressure gradient and that of the potential temperature is in the same direction. As a result, in this region isopycnal stirring requires an external

source of mechanical energy (Fig. 25).

### 3.8 Remark

According to the common wisdom, isopycnal mixing is free of energy. For a long time this is a statement without solid and careful proof. In this section we have gone through careful analysis and show that it is not an accurate statement; in fact, isopycnal eddy diffusion can lead to GPE changes in the mean state. Thus, isopycnal eddy diffusion is not energy free, and energetics of isopycnal eddy diffusion should be carefully analyzed. Furthermore, GPE balance associated with isopycnal eddy diffusion should be used as a tool in the study of isopycnal eddy diffusion and its parameterization.

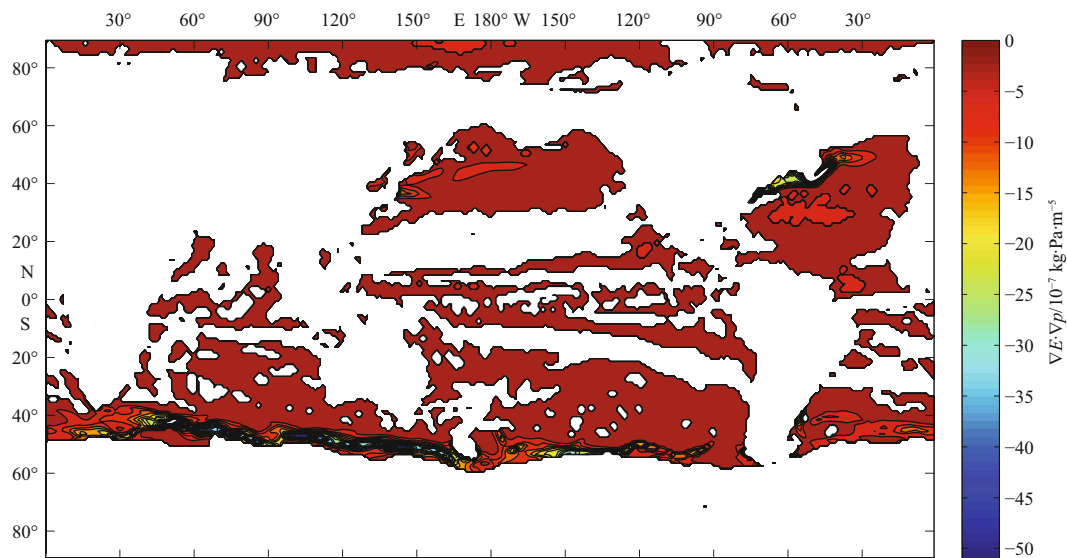


Fig.24. The gradient product of elasticity and pressure, negative values only (based on WOA01) ( $\sigma_{0.5}=29.3 \text{ kg/m}^3$ ).

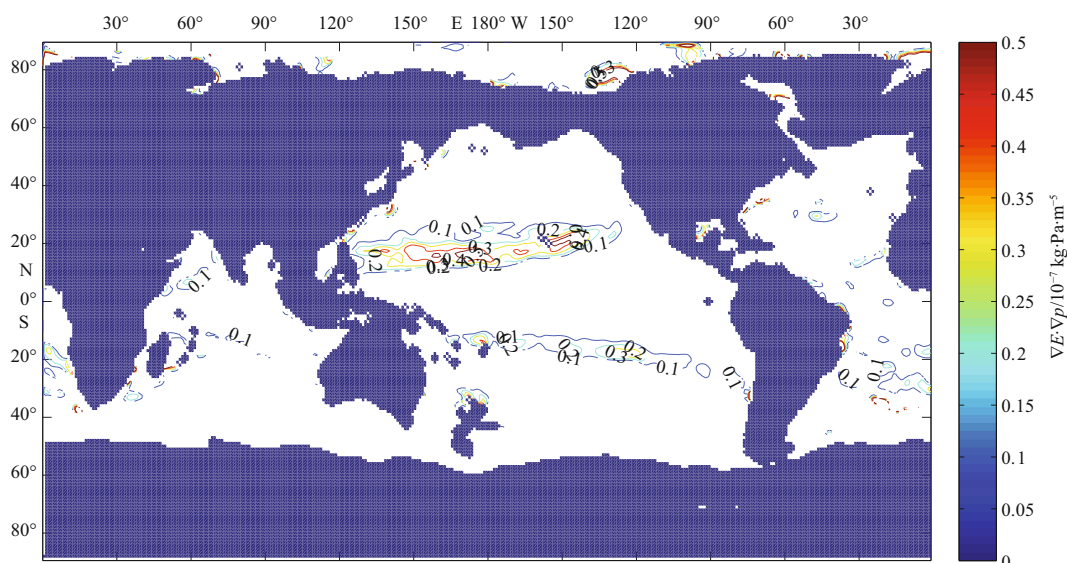


Fig.25. The gradient product of elasticity and pressure, positive values only (based on WOA01) ( $\sigma_{0.5}=29.3 \text{ kg/m}^3$ ).

### Acknowledgement

This study took more than three years to finish. During this long period of time, I received persistent encouragement from many of my colleagues. In particular, Quanan Zheng provided the most need support and suggestions; Kun Xu and Jianping Gan introduced me to the new idea behind the Hui transformation and its application to the unified coordinate; Yihua Lin and Yu Zhang provided very stimulating input to the physics of thermobaric instability and the numerical diffusivity introduced in the Eulerian coordinates. I take this opportunity to thank all my colleagues who gave the most needed support.

### References

- Bryan F. 1987. Parameter sensitivity of primitive equation ocean circulation models. *J Phys Oceanogr*, 17: 970–984
- Carton J A, Giese B S. 2008. A reanalysis of ocean climate using simple ocean data assimilation (SODA). *Mon Weather Rev*, 136: 2999–3017
- Conkright M E, Locarnini R A, Garcia H E, et al. 2002. World Ocean Atlas 2001: Objective analysis, data statistics, and figures, CD-ROM Documentation. National Oceanographic Data Center, Silver Spring, MD, 17
- Eden C, Willebrand J. 1999. Neutral density revisited. *Deep-Sea Res Pt II*, 46: 33–54
- Forster T D, Carmack E C. 1976. Frontal zone mixing and Antarctic bottom water formation in the southern Weddell Sea. *Deep-Sea Res*, 23: 301–317
- Gent P R, McWilliams J C. 1990. Isopycnal mixing in ocean circulation models. *J Phys Oceanogr*, 20: 150–155
- Huang R X. 2014. Energetics of lateral eddy diffusion/advection: Part I. Thermodynamics and energetics of vertical eddy diffusion. *Acta Oceanol Sin*, 33 (3): 1–18
- Hui W H. 2007. The unified coordinate system in computational fluid dynamics. *Commu Compu Phys*, 2: 577–610
- Hui W H, Li P Y, Li Z W. 1999. A unified coordinate system for solving the two-dimensional Euler equations. *J Comput Phys*, 153: 596
- Hui W H, Kudriakov S. 2001. A unified coordinate system for solving the three-dimensional Euler equations. *J Comput Phys*, 172: 235
- Hui W H, Xu K. 2012. Computational Fluid Dynamics Based On The Unified Coordinates. Beijing: Science Press, 198
- McDougall T J. 1987a. Neutral surfaces. *J Phys Oceanogr*, 17: 1950–1964
- McDougall T J. 1987b. The vertical motion of submesoscale coherent vortices across neutral surfaces. *J Phys Oceanogr*, 17: 2334–2342
- McDougall T J. 1987c. Thermobaricity, cabbeling, and water-mass conversion. *J Geophys Res*, 92: 5448–5464
- Nycander N. 2011. Energy conversion, mixing energy, and neutral surfaces with a nonlinear equation of state. *J Phys Oceanogr*, 41: 28–41
- Ledwell J R, Watson A J, Law C S. 1998. Mixing of a tracer in the pycnocline. *J Geophys Res*, 103: 21499–21529
- Lumpkin R, Treguier A-M, Speer K. 2002. Lagrangian eddy scales in the Northern Atlantic Ocean. *J Phys Oceanogr*, 32: 2425–2440
- Obuko A. 1971. Oceanic diffusion diagrams. *Deep-Sea Res*, 18: 789–802
- Qian Y-K, Peng S, Li Y. 2013. Eulerian and Lagrangian statistics in the South China Sea as deduced from surface drifters. *J Phys Oceanogr*, 43: 726–743
- Ruddick B, Kerr O. 2003. Oceanic thermohaline intrusions: theory. *Progr Oceanogr*, 56: 483–497
- Ruddick B, Richards K. 2003. Oceanic thermohaline intrusions: observations. *Progr Oceanogr*, 56: 499–527
- Spivakovskaya D, Heemink A W, Deleersnijder E. 2007. Lagrangian modelling of multi-dimensional advection-diffusion with space-varying diffusivities: theory and idealized test cases, 57(3): 189–203
- Wagner D H. 1987. Equivalence of Eulerian and Lagrangian equations of gas dynamics for weak solutions. *J Differ Equations*, 68: 118–136
- Zheng C, Wang P P. 1999. MT3DMS: a modular three-dimensional multispecies transport model for simulation of advection, dispersion and chemical reactions of contaminants in groundwater systems; documentation and user's guide. Alabama Univ University